Gas permeation in bi-soft segment poly(ester urethane urea) membranes for Membrane Blood Oxygenators

Gabriela Pon

Thesis to obtain the Master of Science Degree in

Chemical Engineering

Supervisors:
Dr. Mónica Cristina Faria Besteiro
Dr. Pedro Jorge Rodrigues Morgado

Examination Committee

Chairperson: Prof. Carlos Manuel Faria de Barros Henriques
Supervisor: Dr. Mónica Cristina Faria Besteiro
Member of the Committee: Prof. Moisés Luzia Gonçalves Pinto

November 2018

Acknowledgements

I would like to express my very great appreciation to my supervisors Dr. Pedro Morgado and Dr. Mónica Faria for their patient guidance, advice and time dedicated to this thesis.

I would like to express my gratitude to Professor Maria Norberta de Pinho for the proposal of this thesis and shared knowledge.

I would like to offer my special thanks to Professor Moisés Pinto, Marta and Marlene for the solubility measurements which was a great contribution to this work.

I am particularly grateful to Tiago for all the help provided which is much appreciated.

Finally, I must express my very profound gratitude to my family and friends who have been a valuable support and motivation throughout my studies. This accomplishment would not have been possible without them.

Abstract

Integral asymmetric and nonporous symmetric poly(ester urethane urea) membranes were synthesized by a modified version of the phase inversion technique and the solvent evaporation technique, respectively, where polyurethane (PUR) and polycaprolactone-diol (PCL) prepolymers were reacted with the solvents dimethyl formamide (DMF) and diethyl ether (DEE). Four casting solutions were prepared with PUR/PCL weight ratio of 90/10, polymer/solvent ratio of 65/35 and DMF/DEE ratios of 3/1 and 1/1, rendering integral asymmetric membranes, A31 and A11, and nonporous symmetric membranes, D31 and D11.

An existing gas permeation setup was optimized by increasing the volume of the receiving chamber and performing vacuum to the setup before the measurements. The results were highly reproducible and permitted the determination of the diffusion and solubility coefficients by the time lag method.

Similar permeances were obtained for the integral asymmetric and nonporous symmetric membranes: 0.12-0.13x10^{-6}cm^3/cm^2.s.cmHg for N_2, 0.32-0.35x10^{-6}cm^3/cm^2.s.cmHg for O_2 and 3.2-3.4x10^{-6}cm^3/cm^2.s.cmHg for CO_2. The permeability coefficients obtained for membrane D31 were: 8, 21 and 208 Barrer for N_2, O_2 and CO_2, respectively. The diffusion coefficients obtained by the time lag method were very similar for the three gases: 7.1-13.0x10^{-7}cm^2/s for N_2, 7.4-11.0x10^{-7}cm^2/s for O_2 and 7.5-12.2x10^{-7}cm^2/s for CO_2. The solubility coefficients obtained by the time lag method were: 0.07-0.08x10^{-2}cm^3/cm^3.cmHg for N_2, 0.20-0.25x10^{-2}cm^3/cm^3.cmHg for O_2 and 1.7-2.2x10^{-2}cm^3/cm^3.cmHg for CO_2, which were the same order of magnitude obtained by the barometric method. The solubility coefficient was found to be the controlling term in these membranes which led to the differences observed in the permeabilities of the gases.

Keywords: Gas permeation; Bi-soft segment polyurethanes; Integral asymmetric membranes; Membrane blood oxygenators; Time lag

Resumo

Membranas integrais assimétricas e membranas densas de poliéster-uretano-ureia foram sintetizadas pelo método de inversão de fase modificado e pelo método de evaporação de solvente, respetivamente, onde se fez reagir pré-polímeros de poliuretano (PUR) e policaprolactona-diol (PCL) em uma mistura de solventes de dimetilformamida (DMF) e dietiléter (DEE). Foram preparadas quatro soluções de casting com as razões mássicas PUR/PCL de 90/10, polímero/solvente de 65/35 e DMF/DEE de 3/1 e 1/1, originando membranas integrais assimétricas, A31 e A11, e membranas densas, D31 e D11.

Uma instalação existente de permeação gasosa foi otimizada por aumento de volume do permeado e por aplicação de vácuo à instalação antes de cada ensaio. Os resultados obtidos foram altamente reprodutíveis e permitiram a determinação dos coeficientes de difusão e de solubilidade pelo método do time-lag.

Foram obtidas permeâncias parecidas para as membranas integrais assimétricas e membranas densas: 0.12-0.13x10^{-6}cm^{3}/cm^{2}.s.cmHg para N_2, 0.32-0.35x10^{-6}cm^{3}/cm^{2}.s.cmHg para O_2 e 3.2-3.4x10^{-6}cm^{3}/cm^{2}.s.cmHg para CO_2. Os coeficientes de permeabilidade obtidos para a membrana D31 foram: 8, 21 e 208 Barrer para N_2, O_2 e CO_2, respetivamente. Os coeficientes de difusão obtidos pelo time lag foram semelhantes para os três gases: 7.1-13.0x10^{-7}cm^{2}/s para N_2, 7.4-11.0x10^{-7}cm^{2}/s para O_2 e 7.5-12.2x10^{-7}cm^{2}/s para CO_2. Os coeficientes de solubilidade obtidos pelo time lag foram: 0.07-0.08x10^{-2}cm^{3}/cm^{3}.cmHg para N_2, 0.20-0.25x10^{-2}cm^{3}/cm^{3}.cmHg para O_2 e 1.7-2.2x10^{-2}cm^{3}/cm^{3}.cmHg para CO_2, o que se encontra na mesma ordem de grandeza que os resultados obtidos pelo método barométrico. Observou-se que o coeficiente de solubilidade é o termo que controla a permeação dos três gases nestas membranas.

Palavras-chave: Permeação gasosa; Poliuretanos com dois segmentos flexíveis; Membranas assimétricas integrais; Oxigenadores de membrana; Time lag

Contents

List of Figures

List of Tables

List of Abbreviations and Symbols

CPB – Cardiopulmonary bypass
ECMO – Extracorporeal membrane oxygenation
PIM – Polymer of intrinsic microporosity
PTMSP – Poly(1-trimethylsilyl-1-propyne)
PU - Polyurethane
PP – Polypropylene
PMP - Polymethylpentene
P - Permeability coefficient
D – Diffusion coefficient
S - Solubility coefficient
J - Volumetric flux
C - Concentration
l – Membrane thickness
p_f – Feed pressure
p_p – Permeate pressure
α – Selectivity
t – Time
A – Effective membrane area
V – Volume
t_{lag} – Time lag
PPO – Poly(propylene oxide)
PUR – Polyurethane prepolymer
PCL – Polycaprolactone diol prepolymer
DMF – Dimethylformamide
DEE – Diethyl ether
SEM – Scanning electron microscopy
PfT – Feed pressure sensor
PpT – Permeate pressure transmitter
σ – Standard deviation
r – Radius of the tube
λ – Mean free path
R – Ideal gas constant
T – Temperature
n – Number of moles
TMP – Transmembrane pressure
$Perm$ – Permeance

1 Introduction

1.1 The human respiratory and cardiovascular systems

The human respiratory system consists of the lungs and the airways: mouth, nose, pharynx, larynx, trachea, bronchi and bronchioles. Its main function is to allow gas exchange between air and blood: oxygen (O_2) from the air enters the blood while carbon dioxide (CO_2) is released from the blood to the air. The cardiovascular system, which consists of the heart and blood vessels, supplies O_2 and nutrients to the whole body. O_2 is essential for cellular respiration in order to produce energy to keep the body functioning. CO_2 is produced as a waste molecule and its removal is important to maintain the pH of the blood.

Gas exchange occurs between the alveoli, which are tiny sacs present in the lungs, and the pulmonary capillaries. In the alveoli, the partial pressures of O_2 and CO_2 are usually 105 mmHg and 40 mmHg, respectively. After gas exchange, the partial pressures of these gases in the blood delivered to the lungs are estimated to increase from 40 mmHg to 100 mmHg for O_2 and decrease from 46 mmHg to 40 mmHg for CO_2. Diffusion of gas is fast as there is an estimated 300 million alveoli, that yields a huge surface area of gas exchange of 60-80 m^2, and each alveolous is surrounded by a big number of capillaries. Furthermore, the distance between the air in the alveoli and the blood in the capillaries is only 2-cell thick (an alveolar cell and a capillary endothelial cell), corresponding to about 0.3 µm.

In an adult at rest, the average cardiac output, which is the volume of blood pumped by the heart, is about 5.5 L/min. The total blood volume is about 5.5 L, which means it takes about a minute for a drop of blood to complete the systemic and pulmonary circuits [1].

1.2 The extracorporeal membrane oxygenation system

According to the World Health Organization, heart diseases have remained the world´s number one top cause of death in the last 15 years. Respiratory diseases are also the leading cause of death, after heart diseases [2].

Cardiopulmonary bypass (CPB), a major development in clinical medicine that occurred in the 1950s, is a form of extracorporeal circulation in which a heart-lung machine temporarily (hours) takes over the normal physiologic functions of the heart and lungs during open heart surgeries, including circulation of blood, oxygenation and ventilation. It allowed surgeons to correct cardiac defects, replace diseased valves, bypass obstructed coronary arteries and perform transplants on a heart that is not beating and in a bloodless environment. Extracorporeal membrane oxygenation (ECMO) is an extension of CPB. It provides a longer-term support which can go on from days to weeks. ECMO allows patients to survive and heal from cardiopulmonary surgery, traumatic injury, infection or inflammation of the lungs and is also used as a bridge to lung transplant. As shown in Figure 1, the ECMO circuit mainly consists of a tubing that takes out the deoxygenated blood from the patient, a pump, an artificial lung, a heat exchanger and a tubing that returns the oxygenated blood to the patient. It is in the artificial lung, also referred to as Membrane Blood Oxygenator (MBO), where gas exchange occurs. Venous-venous cannulation is used for isolated respiratory failure, requiring native heart function, while venous-arterial cannulation is used for cardiac failure, with or without respiratory failure [3,4,5]. The present work is focused on the development of new membranes for MBOs.

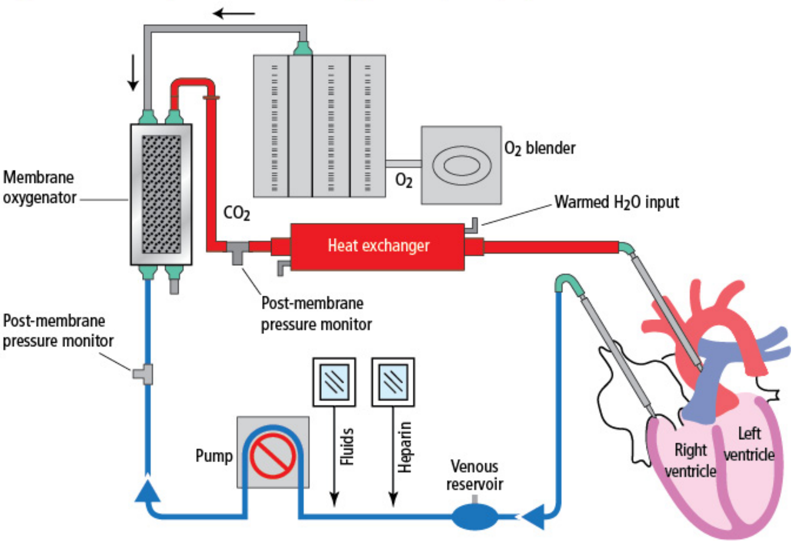

Figure 1 - Extracorporeal membrane oxygenation system [6]

1.3 Membrane Blood Oxygenators

The first successful cardiopulmonary bypass operation was performed in 1953 by Gibbon [7], with a film type oxygenator, which involved a blood film directly exposed to atmosphere. Later, bubble oxygenators were developed, where gas bubbles were directly introduced into the blood. The major breakthrough in blood oxygenation was the development of MBOs, where there is no direct contact between the blood and the O_2, as they are separated by a membrane. This minimized the risk of air embolism [8]. Clowes and Hopkins were pioneers in using a MBO in heart surgery in 1955 [9].

The ideal MBO should be able to [8]:

- Perform efficient gas exchange;
- Be hemocompatible, avoiding hemolysis and protein denaturation;
- Oxygenate up to 5 L/min of venous blood to 95-100% haemoglobin saturation for periods between some minutes till several hours;
- Simultaneously, remove a certain level of CO_2 to avoid respiratory acidosis but also not too much to avoid alkalosis;
- Have reasonable blood priming volume (1-4L);

- Be simple and safe to use, clean and sterilizable.

As shown in Figure 2, the MBO must deliver about 250 cm^3 (STP)/min of O_2 and remove about 200 cm^3 (STP)/min of CO_2. Blood flows of 2-4 L/min are required.

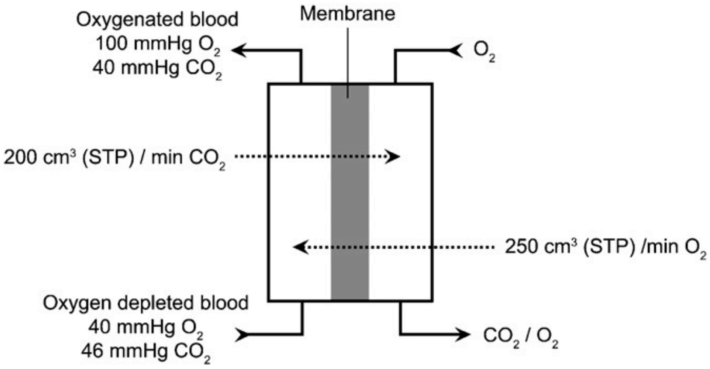

Figure 2 – Principle of the membrane blood oxygenation [8]

2 Literature Review

2.1 Membrane gas separation

Membranes for gas separation have been known for more than a century, however, it was first implemented on an industrial scale in 1980 by Monsanto, for hydrogen separation from the purge gas stream of ammonia plants. Membrane gas separation has, since then, grown rapidly and has become a competitive separation technology. It is a pressure-driven process and is based on physical and/or chemical interactions between the gases and the membrane material. It is considered to be cost-effective, simple to operate, energy-efficient and environmentally friendly [10].

Although numerous new membrane materials have been investigated and developed for gas separation, only a few remain in current commercial use. All of the membranes are polymeric and most of them have been used for decades [11]. Cellulose acetate, polysulfone and polyimides are some of the most important polymers for gas separation membranes. Polymers cannot withstand high temperatures and aggressive chemical environments. Additionally, many polymers become plasticized when exposed to hydrocarbons or CO_2. In general, polymers undergo a trade-off limitation between permeability and selectivity: as selectivity increases, permeability decreases and vice-versa [12].

Other membrane materials include inorganic membranes, hybrid membranes and polymers of intrinsic microporosity (PIM) [13].

Inorganic membranes are interesting due to their ability to resist harsh environments [12]. An appealing membrane of this type is the carbon molecular sieve. Despite much research, it did not find its way to industrial use due to the inherent brittleness of carbon materials, high price and aging of the carbon surface by chemical surface reactions. Another interesting material is the ceramic membrane, known to be a good conductor of O_2 at high temperatures, which is attractive for air separation [13].

Hybrid membranes, often referred to as mixed matrix membranes, are a way to enhance the properties of polymeric membranes by incorporating inorganic material in the form of micro or nanoparticles into a polymeric matrix. Some of the important challenges are their cost, difficulties for commercial scale manufacturing and brittleness. Regardless of these problems, these membranes are on the brink of practical application [12,13].

Polymers of intrinsic microporosity were introduced by Budd *et al* [14]. The molecular structure contains sites of contortion within a rigid backbone conferring it high free volumes. PIMs showed great gas separation abilities, however, long-term measurements revealed aging problems. Research in this area is expected to remain attractive [13].

2.1.1 Current and emerging applications in membrane gas separation

2.1.1.1 Blood oxygenators

Polymeric membranes are used as components in medical devices such as blood oxygenators. In this case, there is no separation of gases but exchange of gas with blood occurs instead, allowing O_2 to enter the blood while CO_2 is removed from the blood. Thus, the membrane serves as a barrier between the blood and the O_2 to prevent direct contact, which can cause air embolism. This application will be further described below in section 2.2.

2.1.1.2 Separation of CO_2 from Natural Gas

CO_2 must be removed from natural gas to meet the pipeline specification of <2%, since it reduces the heating value of natural gas, induces corrosion and freezes at a relatively high temperature, forming dry ice blocks which can cause damage to the equipment. Currently, most separation plants use amine absorption technology and membrane technology based on cellulose acetate. Although operations with amine absorber-strippers is harder and more expensive, it can easily achieve an almost complete separation of CO_2 and a less than 1% loss of CH_4 in the feed to the permeate stream. Current cellulose acetate membranes, with reported CO_2 permeability of 8.9 Barrer and CO_2/CH_4 selectivity of 21 [15], are no match to this performance due to high loss of CH_4 (2-4%). Therefore, membranes with higher CO_2/CH_4 selectivities are needed [11].

Polyimides are the most investigated alternative to this application as they have been reported to have higher selectivities, however, plasticization by CO_2 and other components in natural gas is the main problem [16]. Various cross-linking methods have been attempted to improve resistance to plasticization [17,18]. Other types of materials investigated are PIMs [19] and mixed matrix membranes [20].

2.1.1.3 Air separation

Air separation is considered very difficult because of the small difference in size between N_2 and O_2. N_2 is used in many applications related to safety. Technologies for this separation include cryogenic distillation, pressure swing adsorption (PSA) and membranes. Present materials for membrane processes, such as polysulfone (Air Products), polyimides (Air Liquide, Ube), polycarbonates (Generon) and poly(phenylene oxide) (Aquilo) have O_2/N_2 selectivities of 6-8 and are capable of producing purities of 99% N_2. According to Baker, the impact of improvements in O_2/N_2 selectivity on N_2 production costs has reached a point of diminishing returns [11].

As for O_2 production, membrane processes are still underdeveloped to acquire purities higher than 90%, which are easily achieved by other conventional technologies. However, membranes can be used to produce oxygen enriched air (25-35% O_2), used in industrial furnaces and burners, the medical field, etc [12]. In this case, high permeabilities are needed but selectivities in the range of 2.5-3.5 are sufficient. Polymers such as silicone rubber, ethyl cellulose and polyacetylenes have been used [11]. In order to obtain higher O_2 purities, other materials are being developed, such as modified PIMs [21] and ceramic membranes [22].

2.1.1.4 H_2 separations

The first large-scale application of membrane separation process was developed by Monsanto (now Air Products), in 1980, and it has been a successful alternative to PSA and cryogenic distillation. It consists in H_2 recovery from ammonia purge gas, in which H_2 is separated from N_2, Ar and CH_4. The membrane utilized is a bisphenol-A polysulfone hollow fiber coated with a thin layer of silicone rubber. Later, they were also applied for H_2/CO ratio adjustment of syngas and H_2 recovery in refinery hydrotreaters (H_2/CH_4). Polyimide membranes (Ube, Air Liquide) are currently used for H_2 recovery in refineries (H_2/N_2) [23,12]. Nowadays, there is little motivation for development of better materials [11].

2.1.1.5 Vapor/gas separation

Vapor/gas separation by membranes is growing quickly at the industrial level as it deals with the recovery of valuable organic vapors and off-gas treatment. Some of the main industrial applications are polyolefin plant resin degassing, gasoline vapor recovery systems at large terminals and polyvinyl chloride manufacturing vent gas [12]. Membranes made of silicone rubber are used because the solubility term is controlling, leading to high permeation of vapors. However, higher selectivities are still desired in order to lower operating costs [11]. This has led to the development of other materials such as poly(1-trimethylsilyl-1-propyne) (PTMSP) [24], PIM [25] and ultra-thin MFI (Modernite Framework Inverted) zeolite membranes [26]. PTMSP was later found to have poor chemical resistance to hydrocarbon liquids, which prevented its use in this application [27].

2.1.1.6 Olefin/paraffin separation

Light olefins such as ethylene and propylene are of great importance to petrochemical industries. They are mainly used to produce polyethylene and polypropylene. Olefin/paraffin separation is currently performed by cryogenic distillation because of their similar boiling points, which is highly energy-intensive. Alternative technologies have been examined, like extractive distillation, physical and chemical adsorption/absorption, but were found to be unfeasible [28]. Membranes have been intensively researched. Facilitated transport membranes (FTM), which consists of a carrier (typically metal ions) with a special affinity toward a target gas molecule, have shown good permeability and selectivity required for this separation. However, they showed stability issues [29]. Other examples of investigated materials are glassy polymers [30], mixed matrix membranes [31] and carbon molecular sieves [32].

2.1.1.7 Carbon capture

CO_2 emissions are a product of fossil fuels combustion which are widely used in electric power plants, industrial processes and transportation. Due to its contribution to global warming, methods to reduce its emissions are being developed. One approach that shows to be promising is carbon capture and sequestration (CCS), which aims to capture CO_2 from power plants emissions and sequestrate it into geologic formations for thousands of years [33]. For power production processes, there are three potential locations for carbon capture: post-combustion, pre-combustion and oxy-combustion [23].

Post-combustion capture involves separation of CO_2 from N_2 downstream of the combustion process. Due to low concentration of CO_2 at atmospheric pressure in the flue gas (less than 15%), membranes with high selectivities (estimated CO_2/N_2 selectivity of ≈100) are required to compete with other technologies such as amine absorption [23]. Various membranes based on poly(ethylene oxide) have been investigated. Another approach that allows selectivities higher than polymers is to incorporate amine groups within the polymer matrix for a facilitated transport effect [11,34].

Pre-combustion capture involves the initial conversion of fossil fuel into H_2 and CO_2. Afterwards, CO_2 is removed prior to combustion, which would happen at high pressures (up to 7 Mpa ΔP) and temperatures (300-700 ºC) [12]. Polybenzimidazole based membranes have shown potential for this separation [35].

Oxy-combustion carbon capture is a challenging application as it requires high purity O_2, which produces less flue gas than air-fueled combustion and consists mainly of CO_2 and H_2O [12]. As mentioned earlier in ¨Air separation¨ section, current membranes cannot achieve the required purities.

2.2 Membranes for MBOs

Nowadays, hollow fiber membrane oxygenators have become the standard of care for CPB and bedridden ECMO. A representative device of the hollow fiber technology, the Maquet Quadrox, is shown in Figure 3. Microporous polypropylene (PP) hollow fiber membrane oxygenators have gained popularity, as it brought numerous advantages such as low priming volume, smaller surface area, ease of priming, low transmembrane pressure and adequate gas exchange. However, they present a major disadvantage when it comes to long-term usage, which is plasma leakage through the micropores and, consequently, a decrease in gas exchange. Recently, a non-microporous hollow fiber oxygenator made from polymethylpentene (PMP) was released, which considerably decreased the plasma leakage occurrence [5,36].

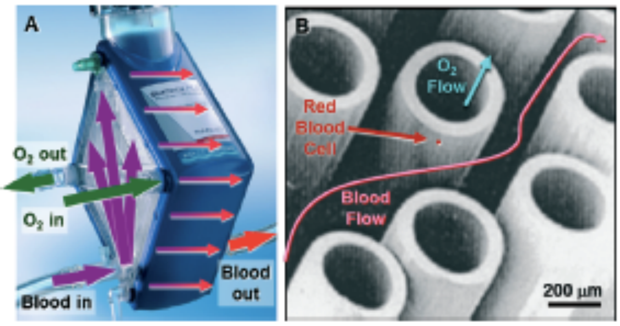

Figure 3 - Current hollow-fiber artificial lung technology. A. Diagram of the Maquet Quadrox. B. Cross-section of the gas-diffusion interface in hollow-fiber artificial lungs. [37]

Currently, many studies are being carried out to improve the hemocompatibility of membranes. Although anticoagulants are used, deposition of blood proteins may still occur after a few days, leading to device failure. In addition, the use of anticoagulants increases the risk for bleeding. In the present, most studies are focused on membrane surface modification/functionalization to enhance hemocompatibility.

Pflaum *et al*. established an endothelial cell monolayer onto PMP membranes. Due to its strong hydrophobic nature, it was previously coated with titanium dioxide using the pulsed vacuum cathodic arc plasma deposition technique, enabling cell adhesion. The monolayer showed no inflammation or thrombus and was able to mend non-seeded or wounded areas under physiological levels of flow-induced shear stress [38].

Wang *et al*. studied the hemocompatibility of a PP hollow fiber membrane coated with a crosslinkable zwitterionic copolymer. The hemocompatibility was evaluated by animal extracorporeal blood circulation and it showed significant resistance to protein adsorption and activation of blood components [39].

On the other hand, microfluidic artificial lungs are being developed with the intention of providing significant advantages in terms of gas exchange, portability and biocompatibility compared to current alternatives. It promises to reduce the surface area and priming volume (to improve patient outcomes and reduce device size), to provide more natural blood flow paths (to improve hemocompatibility) and enable more natural ventilation (using air instead of pure oxygen). The main challenges that remain before it can be clinically used are the large-scale manufacturing and the long-term hemocompatibility [37]. A conceptual drawing of one possible initial clinical implementation of microfluidic artificial lung technology is shown in Figure 4.

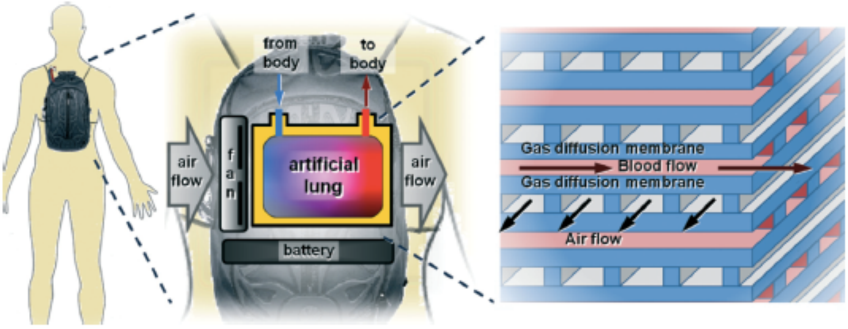

Figure 4 - Conceptual drawing of an initial clinical application of microfluidic artificial lung technology [37]

2.3 Polyurethanes in biomedical applications

Polyurethane (PU) materials were first introduced in biomedical applications in the late 1950s. Due to their outstanding mechanical properties and biocompatibility, they are being widely used in tissue engineering, orthopedic implants, transdermal patches and drug delivery carriers. It has been the top material candidate for biomedical devices for cardiovascular applications such as catheters, pacemaker leads insulation, vascular prostheses, heart valves, cardiac assist devices, etc. Despite this, much research is still being done to expand the applications of PUs or to optimize its properties to meet the demands of certain applications [40].

In terms of biocompatibility, it was found that blood biocompatibility of PUs is related to surface morphology [41]. Hard segments of PUs were found to be highly thrombogenic in platelet retention experiments [42] and crystallinity degree, hydrophobicity, surface free energy and urethane linkage content caused platelet adhesion [43]. Based on these results, surface modification has been done to improve the biocompatibility of PUs, such as incorporation of nanocomposites [44] and bioactive glass [45].

Biostability of PUs has been another main concern, therefore most PU medical devices were used as short-term implants only. It is known that polyester based PU is not stable in water and oxygen, so most PUs used are either polyether or polycarbonate based. To improve the biostability of PUs, many modification efforts were made, such as replacing the soft segment of PU with more stable materials, like polysiloxane [46], and surface modification by incorporation of nanocomposites [47]. Although biostability is very important for long-term medical devices, biodegradable PUs are desired in other applications such as drug delivery, short-term implants, wound dressings, scaffolds and so on. Much research has been done recently on drug-controlled release, due to the significant advantages it brings compared to traditional administration of drugs, such as lower toxicity, less side effects, fewer injection administrations and so on [40]. The use of PUs embedded with carbohydrates has been a recent research trend for enhancement of biocompatibility, biodegradability and PU properties [48].

2.4 Polyurethane membranes for MBOs

Zhao and de Pinho [49] have synthesized bi-soft segment poly(ester urethane urea) membranes by introducing poly(butadienediol) (PBDO) as a second soft segment. The introduction of another soft segment further increases the versatility in the structure design of PU membranes due to different degrees of phase separation between the two soft segments and different degrees of phase segregation between the hard and soft segments. Studies by Queiroz and de Pinho [50,51] showed that a membrane containing 20 wt.% of PBDO had higher degree of cross-linking, showed phase separation of the two soft segments and had higher CO_2 permeability, dependant on the feed pressure, which ranged from 150 to 950 Barrer. A membrane containing 67 wt.% of PBDO had lower degree of cross-linking, was more homogeneous, as the two soft segments were highly dispersed in each other, and lower CO_2 permeability, which was also dependant on the feed pressure and ranged from 90 to 550 Barrer. It was reported that the increase of PBDO content in the membranes increases the mixing of the two soft segments and decreases the aggregation of the hard segments (urethane/urea groups).

The same group has synthesized bi-soft segment poly(ester urethane urea) membranes by introducing another soft segment, which is the polydimethylsiloxane (PDMS) [52]. Studies revealed that the membranes with PDMS content ranging from 25 to 75 wt.% showed phase separation of the two soft segments and that the hard segments form small aggregates somewhere in these two phases. It was also concluded that the increase in PDMS content from 25 to 75 wt.% led to the increase of permeabilities to CO_2 from 200 to 800 Barrer and O_2 from 30 to 120 Barrer. The higher permeability of the membrane containing 75 wt.% was regarded as being caused by the higher fraction of siloxane segments, lower degree of cross-linking and lower aggregation of urethane/urea groups.

Faria *et al*. have introduced polycaprolactone (PCL) as a second soft segment to poly(ester urethane urea) integral asymmetric membranes, which strongly improved the hemocompatibility [53,54,55], compared to the PU/PBDO and PU/PDMS membranes. Although CO_2 permeation fluxes were in the order of magnitude required for commercial membrane oxygenators, the results for O_2 were much below the requirements [56]. The membranes containing PCL content ranging from 0 to 15 wt.% were characterized by infrared spectroscopy and it was concluded that the urethane groups form hard segment aggregates dispersed in the soft segment phase and that this aggregation increases with the increase in PCL content. Gas permeation experiments performed by a photoacoustic system resulted in permeabilities to CO_2 that increased from 188 to 337 Barrer when PCL content increased from 0 to 10 wt.% and was the lowest for 15 wt.% PCL content, which was 113 Barrer. The permeability to O_2 was independent of PCL content and was between 10 and 11 Barrer. Therefore, the membrane that showed the highest CO_2 permeability is the one that contains 10 wt.% PCL and is characterized by the highest contribution of hydrogen bonding between urethane and urea hard segments [57].

Recently, Eusébio [58] built an experimental gas permeation setup capable of recording the evolution of the permeate pressure online at a constant temperature, in intervals of 1.3 seconds, with a precision better than 10 Pa. However, results showed low reproducibility and high uncertainty associated for more permeable membranes, possibly due to various factors such as the small size of the receiving chamber and the fact that vacuum wasn´t applied to the setup prior to the measurements. Furthermore, a transient state was not observed in measurements with O_2, which made it impossible to determine the diffusion and solubility coefficients for this gas by the time lag method. Therefore, the optimization of the gas permeation setup is one of the aims of this work, in order to obtain more precise measurements and to be able to determine the diffusion and solubility coefficients of O_2 and CO_2 by the time lag method.

Eusébio [58] synthesized various bi-soft segment poly(ester urethane urea) membranes with PCL by varying the polymer/solvent ratio, polymers ratio (PUR/PCL), solvents ratio (DMF/DEE) and solvent evaporation time. Gas permeation results for membranes prepared with 1 minute solvent evaporation time were not reproducible and had high uncertainty associated. The membrane that showed the most promising result was the membrane with 1/1 polymer/solvent ratio, 85/15 PUR/PCL ratio and 5 minutes of solvent evaporation time. The N_2, O_2, and CO_2 permeances obtained for this membrane were 0.004 x 10^{-5} $cm^3/cm^2.s.cmHg$, 0.015 x 10^{-5} $cm^3/cm^2.s.cmHg$ and 0.13 x 10^{-5} $cm^3/cm^2.s.cmHg$, respectively. In this work, these bi-soft segment poly(ester urethane urea) membranes containing PCL were synthesized and measured in the optimized gas permeation setup.

3 Framework and thesis objectives

As was revealed in the literature review, enhancement of O_2 permeation properties of bi-soft segment poly(ester urethane urea) membranes and improvement of the gas permeation setup built by Eusébio are required.

The main objectives of this thesis are:

1) Synthesis of integral asymmetric and nonporous symmetric poly(ester urethane urea) membranes with PCL as a second soft segment and characterization by scanning electron microscopy (SEM);
2) Optimization of an existing gas permeation setup in order to improve the precision of gas permeability measurements;
3) Experimental determination of O_2 and CO_2 permeabilities, diffusion and solubility coefficients of the synthesized membranes.

4 Mass Transport Phenomena

4.1 Solution-diffusion model

The transport of a single gas through a dense, nonporous polymeric membrane can be described by the solution-diffusion model. Being the pressure difference across the membrane the driving force, the gas molecules dissolve in the upstream face of the membrane, diffuse across the membrane and desorb from the downstream face of the membrane. Thus, the permeability (P) is both a function of diffusivity (D) and solubility (S) [10]:

$$P = DS \tag{1}$$

In the steady-state, the unidimensional diffusive flux is described by the Fick´s First Law of diffusion:

$$J_A = -D_A \frac{dC_A}{dx} \tag{2}$$

where J_A is the flux of species A in the x direction and is proportional to the concentration gradient $\frac{dC_A}{dx}$. C_A is the concentration of species A in the membrane and D_A is a proportionality constant defined as the diffusion coefficient. To simplify the calculations, it was assumed that the Knudsen diffusion is controlling, so the diffusion coefficient becomes independent of the concentration. The higher the pressures used, the more invalid is the assumption.

Integrating Equation 2 over the thickness of the membrane, l, gives

$$J_A = \frac{D_A}{l}(C_{A0} - C_{Al}) \tag{3}$$

where C_{A0} and C_{Al} are the concentrations of A in the membrane on the feed side and permeate side, respectively.

The solubility of gases in elastomers is usually very low and can be described by Henry´s Law, given by Equation 4, where the concentration inside the polymer, C, is proportional to the applied pressure, p.

$$C = Sp \tag{4}$$

By applying Henry´s Law, the following relations can be established

$$S_A = \frac{C_{A0}}{p_f} = \frac{C_{Al}}{p_p} \tag{5}$$

where S_A is the solubility coefficient of A, p_f is the pressure of the feed and p_p is the pressure of the permeate [59].

Combining Equations 3 and 5 gives the following expression

$$J_A = \frac{D_A S_A}{l}\left(p_f - p_p\right) \qquad (6)$$

Since the product $D_A S_A$ is equal to the permeability coefficient, P_A, Equation 6 can be written as

$$J_A = \frac{P_A}{l}\left(p_f - p_p\right) \qquad (7)$$

The permeability coefficient is commonly expressed in Barrer where

$$1\ Barrer = 10^{-10}\left(\frac{cm^3(STP)\ cm}{cm^2\ s\ cmHg}\right)$$

When the thickness is difficult to define, the pressure normalized flux or permeance, $\frac{P_A}{l}$, is used instead.

The ideal selectivity of the membrane, $\alpha_{A/B}$, is the ratio of the permeabilities or permeances of the individual gases. For a mixture of gas A and B the ideal selectivity is described by [10]:

$$\alpha_{A/B} = \frac{P_A}{P_B} \qquad (8)$$

4.2 Time-lag method

In the transient-state, the mass balance of the unidimensional diffusive transport of species A through a dense, nonporous polymeric membrane is given by the following expression:

$$-\frac{dC_A}{dt} = \frac{dJ_A}{dx} \qquad (9)$$

Substituting the flux by the Fick´s First Law (Equation 2), the Fick´s Second Law is obtained:

$$\frac{dC_A}{dt} = D_A\frac{d^2C_A}{dx^2} \qquad (10)$$

If the membrane is initially free of the diffusing species, the following initial and boundary conditions for the system can be applied:

$$C_A(x, 0) = 0 \qquad (11.a)$$

$$C_A(0,t) = C_{A0} \qquad (11.b)$$

$$C_A(l,t) = C_{Al} \approx 0 \qquad (11.c)$$

which means that the upstream concentration, C_{A0} , remains constant and the downstream concentration, C_{Al}, is negligible compared to the upstream during the diffusion process. Fulfilling these boundary conditions, the solution of Equation 10, either by Laplace transform or separation of variables, is given by [60,61]:

$$C_A = C_{A0}\left(1-\frac{x}{l}\right)+\frac{2C_{A0}}{l}\times\sum_{n=1}^{\infty}\frac{1}{n}\sin\left(\frac{n\pi x}{l}\right)exp\left(-\frac{D_A n^2\pi^2 t}{l^2}\right) \quad (12)$$

The solution expressed in terms of the diffusive flux can be obtained by substituting Equation 12 in the Fick´s First Law:

$$J_A(x,t) = \frac{D_A C_{A0}}{l}+\frac{2D_A C_{A0}}{l}\times\sum_{n=1}^{\infty}\cos\left(\frac{n\pi x}{l}\right)exp\left(-\frac{D_A n^2\pi^2 t}{l^2}\right) \quad (13)$$

The first term in Equation 13 is the steady state portion of the flux and the second term represents the transient contribution. It is a function of time and displacement in the direction of diffusion and hence can be solved for the fluxes entering and leaving the membrane ($x = 0$ and $x = l$, respectively).

By setting $x = l$, yields a time dependant flux equation relative to the downstream end of the membrane. Integrating it with respect to time, yields the amount of species A permeating out of the membrane, Q_{Al}:

$$Q_{Al}(t) = -A\int_0^t J_A(t)dt = \frac{AD_A C_{A0}}{l}\left[t-\frac{l^2}{6D_A}+\frac{2l^2}{\pi^2 D_A}\times\sum_{n=1}^{\infty}\frac{(-1)^{n+1}}{n^2}exp\left(-\frac{D_A n^2\pi^2 t}{l^2}\right)\right] \quad (14)$$

The permeate pressure is, then, obtained from the amount of species A permeating out of the membrane:

$$p_p(t) = \frac{AD_A p_f}{Vl}\left[t-\frac{l^2}{6D_A}+\frac{2l^2}{\pi^2 D_A}\times\sum_{n=1}^{\infty}\frac{(-1)^{n+1}}{n^2}exp\left(-\frac{D_A n^2\pi^2 t}{l^2}\right)\right] \quad (15)$$

where A is the cross-sectional area available for gas penetration perpendicular to the direction of diffusion and V is the volume of the receiving chamber. The steady-state asymptote of Equation 15 is found by taking the limit as $t \to \infty$, reducing the transient term to zero. The permeate pressure is, then, given by:

$$\lim_{t\to\infty} p_p(t) = \frac{AD_A p_f}{Vl}\left[t-\frac{l^2}{6D_A}\right] \qquad (16)$$

The intercept on the time axis of the plot of pressure rise versus time is defined as the time lag, t_{lag}:

$$t_{lag} = \frac{l^2}{6D_A} \tag{17}$$

From the time lag and knowing the membrane thickness, the diffusion coefficient can be obtained. Therefore, Equations 16 and 17 are the main expressions in this work for the line fitting of the steady state asymptote of the gas permeation curves.

4.3 Early approximation method

A solution to the mass balance of Equation 10 was developed by Rogers *et al*. for the transient state of diffusion, before it reaches the steady state of flow into the receiving volume. This solution is useful for more impermeable materials, which steady state takes more time (hours and possibly weeks) to be reached. The transient flux at the downstream end of the membrane $(x = l)$ is, then, given by [61,62,63]:

$$J_A(t) = 2C_{A0}\sqrt{\frac{D_A}{\pi t}}\sum_{n=0}^{\infty} exp\left(\frac{-(2n+1)^2 l^2}{4D_A t}\right) \tag{18}$$

The terms of the series in Equation 18 are small compared to the first term, therefore by keeping only the first term, the following short time solution is obtained:

$$\lim_{t\to 0} J_A(t) = 2C_{A0}\sqrt{\frac{D_A}{\pi t}} exp\left(-\frac{l^2}{4D_A t}\right) \tag{19}$$

It is suggested that the upper time limit for application of Equation 19 should be 2.7 times the time lag. Integrating Equation 19 from 0 to t, an equation expressed in terms of the pressure in the receiving chamber is obtained:

$$p_p(t) = \frac{p_f S_A RTA}{C_{A0}V}\int_0^t J_A(t)dt = \frac{4p_f S_A RTA}{V}\sqrt{\frac{D_A}{\pi}}\sqrt{t} exp\left(-\frac{l^2}{4D_A t}\right) \tag{20}$$

Equation 20 is then linearized:

$$ln\left(\frac{p_p(t)}{\sqrt{t}}\right) = ln\left(\frac{4p_f S_A RTA}{V}\sqrt{\frac{D_A}{\pi}}\right) - \frac{l^2}{4D_A}\frac{1}{t} \tag{21}$$

By plotting $ln\left(\frac{p_p(t)}{\sqrt{t}}\right)$ versus $\frac{1}{t}$, the diffusion coefficient can be obtained from the slope m:

$$m = -\frac{l^2}{4D_A} \tag{22}$$

5 Optimization of the gas permeation setup

The gas permeation setup built by Eusébio [58] showed low reproducibility and high uncertainty associated for more permeable membranes, possibly due to various factors such as the small size of the receiving chamber and the fact that the setup wasn´t evacuated with a vacuum pump prior to the measurements. Furthermore, a transient state was not observed in measurements with O_2 and N_2, which made it impossible to determine the diffusion and solubility coefficients for these gases by the time lag method.

With the purpose of obtaining more precise gas permeation measurements of membranes, an increase of the volume of the receiving chamber of Eusébio´s setup was done by adding a second cylinder (Cylinder 2) with a volume of 394.9 ± 1.5 cm^3. Also, a vacuum pump was added to evacuate the whole setup before each measurement in order to abide by the initial and boundary conditions, Equations 11.a, 11.b and 11.c, of the Fick´s Second Law of diffusion. The resulting setup (Setup A) is presented in Figure 5.

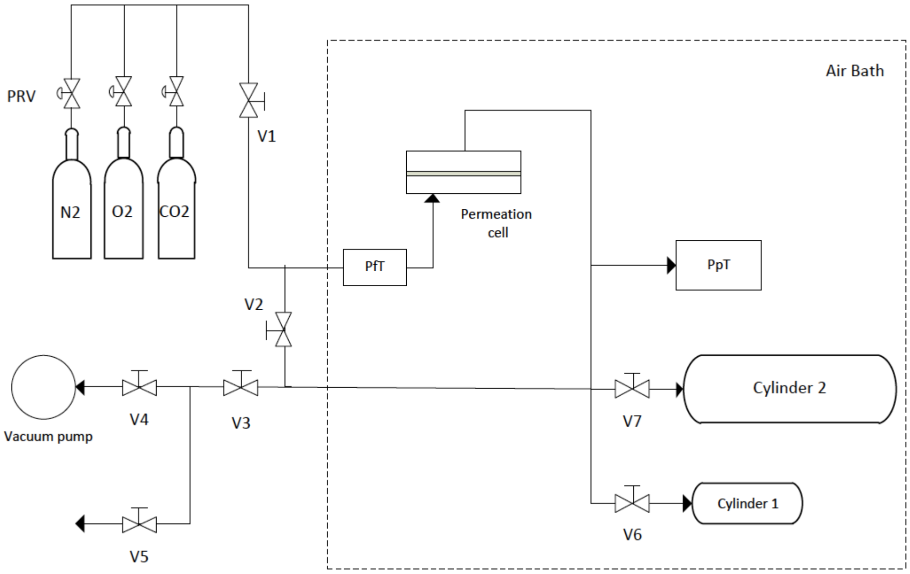

Figure 5 - Schematic representation of the gas permeation setup (Setup A)

Samples of a commercial membrane, taken from a MBO marketed by Avecor/Medtronics, model 0600, were tested with N_2 in the setup A.

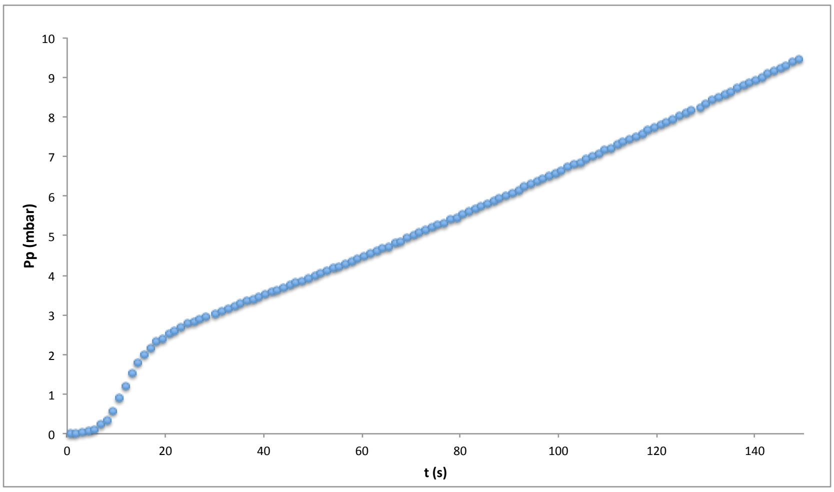

Figure 6 – N_2 permeate pressure vs time for the commercial membrane at a feed pressure of 1.9 bar, obtained in setup A with Cylinder 2 of volume 394.9 cm^3

Figure 6 shows the pressure rise in the permeate side with time for the commercial membrane by feeding N_2 at a pressure of 1.9 bar, in setup A with Cylinder 2 of volume 394.9 cm^3. It can be seen that after about 5 seconds, the pressure rises fast and then slows down at about 15 seconds and gradually reaches a steady state. As a result, the time lag, which is the intersection of the steady state asymptote with the time axis, is negative. Furthermore, the resulting N_2 permeance is $2.17 \pm 0.21 \times 10^{-5}$ cm^3 cm^{-2} s^{-1} cmHg, which is not in agreement with the previously reported result of $0.33 \pm 0.04 \times 10^{-5}$ cm^3 cm^{-2} s^{-1} cmHg obtained by Eusébio´s setup [58]. The occurrence can be explained by the existence of resistance to the transport of gas which prevents its uniform distribution downstream from the membrane leading to a higher concentration of gas near the membrane.

The big cylinder was substituted by a smaller one with a volume of 167.2 ± 0.2 cm^3.

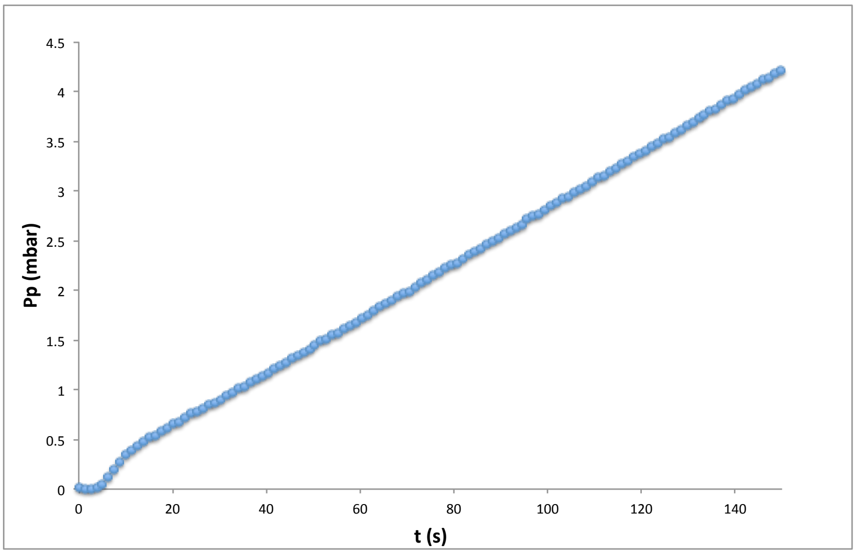

Figure 7 - N_2 permeate pressure vs time for the commercial membrane at a feed pressure of 1.9 bar, obtained in setup A with Cylinder 2 of volume 167.2 cm^3

Observing Figure 7, it can be seen that the pressure still rises fast after 5 seconds and gradually slows down. The time lag is at a value around 0 s. However, the N_2 permeance is 0.34 ± 0.00 x 10^{-5} cm^3 cm^{-2} s^{-1} cmHg, which is in agreement with the previously reported result of 0.33 ± 0.04 x 10^{-5} cm^3 cm^{-2} s^{-1} cmHg [58], which means there was an improvement by substituting the big cylinder, probably because its larger volume amplified the effect of the resistance to the gas transport in the tubes.

Kruczek *et al*. have also observed this situation and have studied various configurations of the permeate side and have developed analytical solutions for the calculation of the effective time lag [64,65,66,67].

This situation is expected to occur in high vacuums, which is required by the time lag method, where the transport of gas molecules is governed by the Knudsen flow, which happens when a gas molecule collides much more frequently with the walls of the tube rather than with other gas molecules. This occurs when the radius of the tube (r) is much smaller than the mean free path of gas molecules (λ). It is common to assume that when $r/\lambda < 0.1$, the gas transport is controlled by Knudsen diffusion.

The mean free path, which is the average distance traveled by a molecule between successive collisions is given by [64]:

$$\lambda = \frac{1}{\sqrt{2}\pi d^2 n} \tag{23}$$

where d is the molecular diameter and n is the molecular concentration given by:

$$n = \frac{pN_A}{RT} \tag{24}$$

where p is the pressure, N_A is the Avogadro´s number, R is the ideal gas constant and T the absolute temperature. From Equations 23 and 24, it is evident that the mean free path is inversely proportional to the pressure.

Figure 8 shows the relationship between the mean free path of N_2 molecules at 300 K and the pressure. Using the criterion $r/\lambda < 0.1$, it also shows the pressures below which the Knudsen flow exists in standard stainless steel tubes of 1/8, 1/4 and 1/2 in., with the respective internal diameters of 0.175, 0.386 and 1.02 cm.

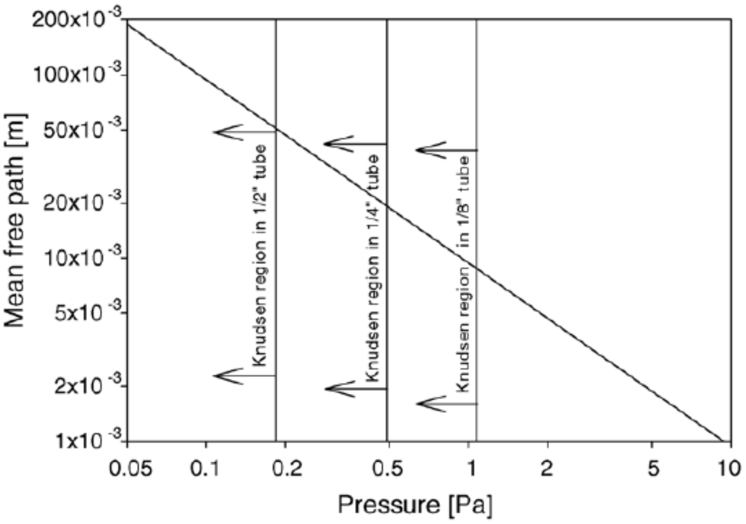

Figure 8 - Effect of pressure on the mean free path of N_2 molecules at 300 K [64]

As the tubes used in the gas permeation setup are of 1/8 in. and according to Figure 8, Knudsen diffusion exists below a pressure of 1 Pa, for N_2 molecules at 300 K. Above this pressure, r/λ increases and the collisions between gas molecules become more frequent and the resistance to accumulation of gas should decrease. However, in this experiment, where the vacuum pump used is capable of reaching pressures below 10 Pa, the resistance to gas transport was observed. Kruczek *et al*. have also observed that even at initial pressures of 5.5 Pa and higher where the transport is not controlled by the Knudsen diffusion, the effect of the resistance still occured.

According to studies by Kruczek *et al*., the resistance to accumulation of gas in the tube is practically negligible, however, the addition of a resistance-free tank in the receiving chamber may greatly amplify the resistance to gas transport in the tube which connects the flow source to the tank and also affect the time lag. It was found that the time lag strongly depends on the position of the pressure sensor, as well as, on the volume of the tank and the position where the tank is connected to the main tube.

To minimize the possible errors, it is suggested that:

- The volume of the tank should not be much greater than the volume of the main tube;
- The volume should be maximized by using tubes of large internal diameter (at least 1/2 in.);
- The tank should be attached as close as possible to the flow source;
- The pressure sensor should never be installed in the main tube before the tank because the closer it is to the flow source the more negative will be the time lag;
- The optimum location of the pressure sensor is in the tank, however, if a single pressure sensor is available, it cannot be installed in the tank. Then, the pressure sensor should be installed towards the end of the main tube, downstream from the point at which the tank is attached to the main tube.

In case of multi-tank receivers:

- The pressure sensor should be installed downstream from the junction to the last accumulation tank;

- It is better to split the total volume of the receiving chamber into several smaller tanks rather than using one large tank;
- Using tanks of similar volumes is recommended;
- While in general the length of tubing in the receiver should be minimized, the most critical is the length of the tubes connecting the accumulation tanks with the main line, followed by the length of tubes in the main line upstream from the junction to the last accumulation tank. On the other hand, the length of branch tubes, which do not connect to the accumulation tanks and the tubes in the main line downstream from the junction to the last accumulation tank, has little effect on the time lag at the end of the main line.

As suggested, the positions of the pressure transmitter (PpT) and Cylinder 1 were switched as shown in Figure 9 (setup B), so that the pressure transmitter is placed at the end of the main tube.

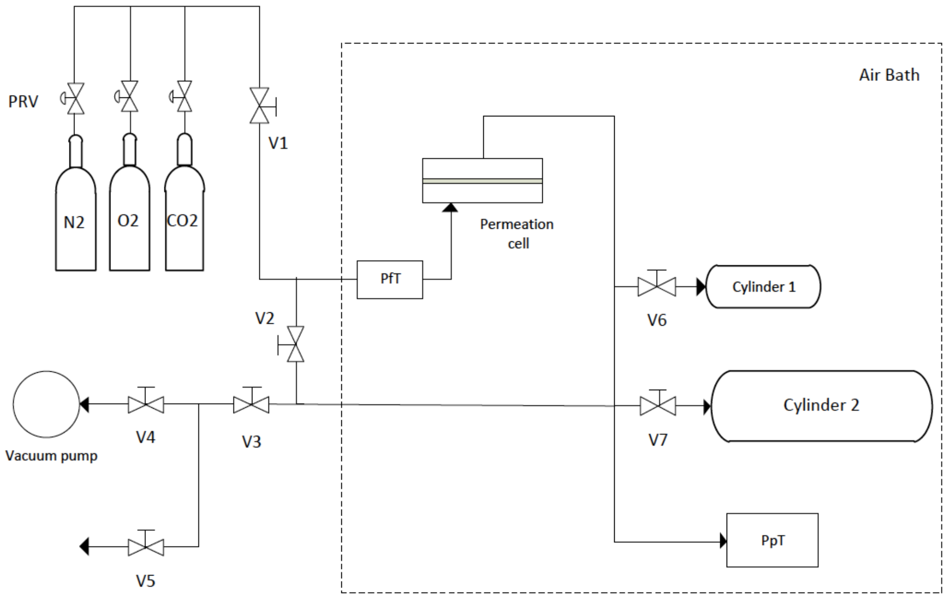

Figure 9 - Schematic representation of the gas permeation setup (Setup B)

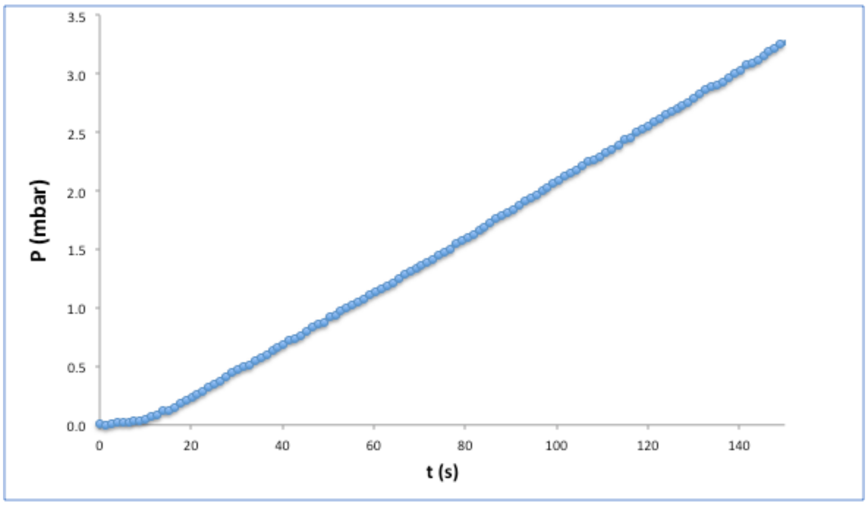

Figure 10 - CO_2 permeate pressure vs time for the A31 membrane at a feed pressure of 1.9 bar, obtained in setup B

As shown in Figure 10, the effect of the resistance to accumulation of gas is no longer shown and it can be seen that in the transient state the pressure gradually rises until reaching the steady state. However, placing the pressure transmitter at the end of the tube could lead to a more positive time lag. To evaluate this effect, two measurements were carried out at initial permeate pressures of 0 and 1 mbar. At 1 mbar, or 100 Pa, the resistance to gas transport should not be measurable and, therefore, the time lag should not be affected. Both permeation curves are represented in Figure 11.

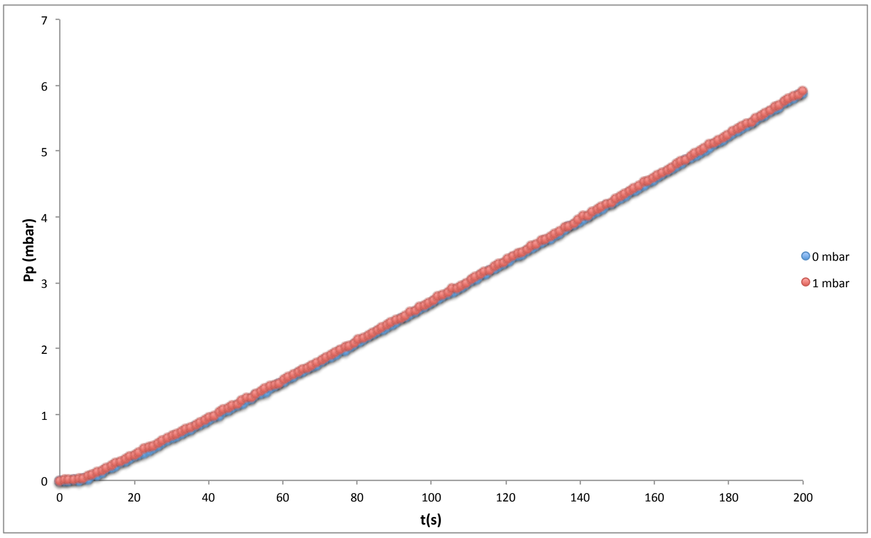

Figure 11 - CO_2 permeate pressure vs time for a poly(ester urethane urea) membrane at a feed pressure of 2.4 bar and initial permeate pressures of 0 mbar (blue) and 1 mbar (red), obtained in setup B

At initial permeate pressures of 0 mbar and 1 mbar, the time lags obtained were 25.17 s and 24.91 s, respectively, corresponding to a relative error of about 1%. Hence, the position of the pressure transmitter did not significantly affect the time lag.

The obtained setup (Figure 9) consists of a permeation cell, a feed pressure sensor (PfT) (Setra, Model 205, Massachusetts, USA), a permeate pressure transmitter (PpT) (Intelligent Transmitter Paroscientific, Series 6000, model 6100A-CE Inc. Washington, USA) attached to a Paroscientific model 710 display unit, which is connected to a computer, a small cylinder with a volume of 12.6 ± 0.1 cm^3 (Cylinder 1), a big cylinder with a volume of 167.2 ± 0.2 cm^3 (Cylinder 2) and a vacuum pump (Edwards E2M2 Rotary Vane Vacuum Pump, UK). The volume of Cylinder 1 was previously calibrated by gravimetry [58], in which the cylinder was filled with a liquid of known density and weighted. The calibration of the volumes of Cylinder 2 and the tubes were done by gas expansion and is presented in Annex 11.1. The tubes in the receiving chamber have a volume of 13.5 ± 0.01 cm^3, resulting in a total volume of the permeate side of 193.3 ± 0.3 cm^3.

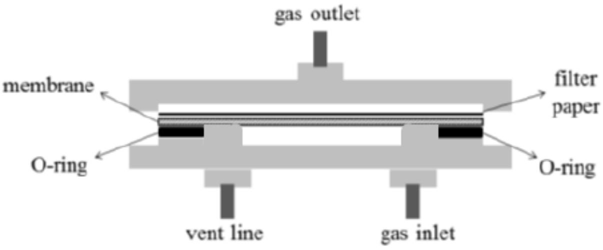

Figure 12 - Schematic representation of the permeation cell

The membrane is sandwiched between two plates of stainless steel in the permeation cell with a surface area of 9.62 cm^2, as shown in Figure 12. The tubing system contains tubes of stainless steel 316 with an external diameter of 1/8 inch (Hoke®), needle valves (3700 Series, Hoke®) and tube fittings made of stainless steel, titanium and brass (Gyrolok®). The equipment was installed in a thermostatic system which consists of a wine fridge (cold source), a resistance thermometer, a heater connected to a PID controller and a fan to homogenize the inner temperature. The variation of the pressure was recorded with the software Digiquartz® version 2.0 (Paroscientific Inc, Washington, USA).

6 Experimental

6.1 Materials

6.1.1 Materials for the synthesis of poly(ester urethane urea) membranes

Two prepolymers were used for the synthesis of the poly(ester urethane urea) membranes: poly(propylene oxide) (PPO) based polyurethane prepolymer with three isocyanate terminal groups (PUR), supplied by Fabrires-Produtos Químicos S.A., and polycaprolactone diol prepolymer (PCL), supplied by Sigma-Aldrich with a stated molecular weight of 530 Da. The solvents used were dimethylformamide (DMF) (p.a. grade, 99.8%) and diethyl ether (DEE) (p.a. grade, 99.5%) provided by Panreac. The catalyst used was stannous octoate (p.a. grade, 95%) provided by Sigma-Aldrich.

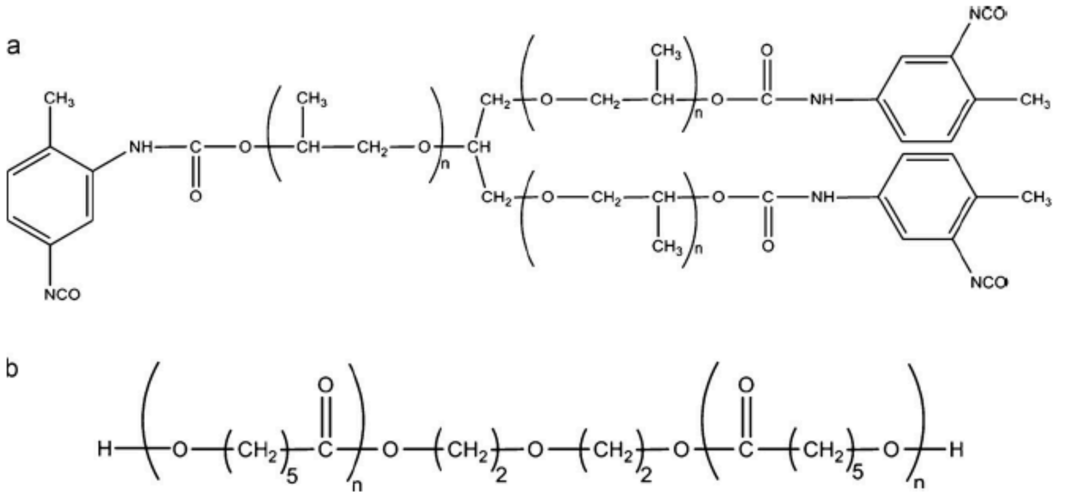

Figure 13 - (a) Chemical structure of the poly(propylene oxide) based prepolymer (PUR) and (b) polycaprolactonediol (PCL) [56]

Membranes synthesized solely with PUR contain one soft segment, PPO, and one hard segment of type I, as shown in Figure 14. Type I is formed by the reaction of two segments of PUR, consisting of two urethane groups linked by two toluene and one urea group. With the introduction of PCL, a second soft segment is formed, along with a second hard segment of type II, as shown in Figure 15. Type II is originated by the reaction of one segment of PUR and one segment of PCL, consisting of two urethane groups linked by one toluene group. This hard segment is shorter than type I.

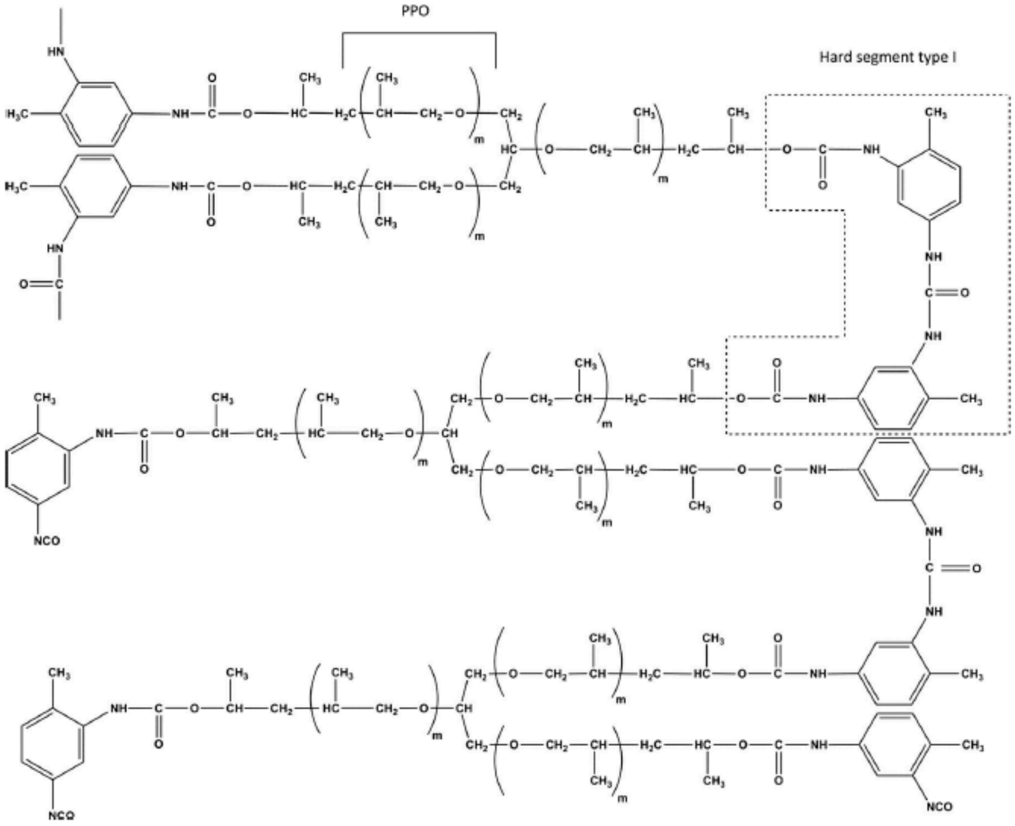

Figure 14 - Chemical structure of the poly(urethane urea) synthesized with PUR and composed of only one soft segment (PPO) and hard segment type I [57]

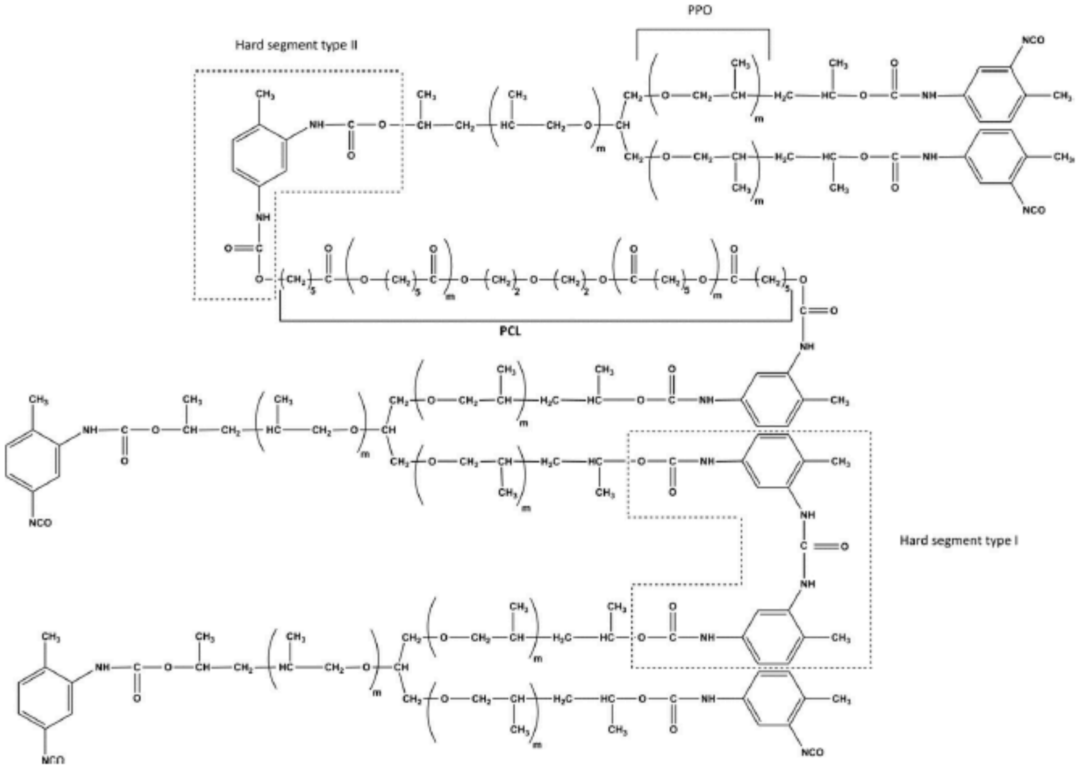

Figure 15 - Chemical structure of the poly(urethane urea) synthesized with PUR and PCL containing two types of soft segments (PPO and PCL) and type I and type II hard segments [57]

6.1.2 Gases

Gas permeation experiments and gas solubility measurements were carried out using nitrogen (purity ≥ 99.999%), carbon dioxide (purity ≥ 99.98%) and oxygen (purity ≥ 99.5%), all supplied by Air Liquide.

6.2 Synthesis of poly(ester urethane urea) membranes

Integral asymmetric poly(ester urethane urea) membranes were synthesized by a modified version of the phase inversion technique [68]. Firstly, two casting solutions were prepared with a PUR/PCL prepolymer weight ratio of 90/10 and a prepolymer/solvent weight ratio of 65/35. The casting solutions differed in the ratio of DMF/DEE solvents used: 3/1 and 1/1. 3-4 drops of catalyst, stannous octoate, were added and the solutions were stirred for about 2 hours at room temperature. In the next step, each solution was spread on a glass plate with a 150 μm casting knife and a solvent evaporation time of 1 minute was applied. After this, the glass plates were placed in a coagulation bath (deionized water) for at least 12 hours. The membranes were then carefully removed from the glass plate, washed with deionized water to remove all solvents and left to dry at room temperature. The resulting membranes were designated A31 and A11, which correspond to DMF/DEE ratios of 3/1 and 1/1, respectively.

Nonporous symmetric membranes were synthesized with the same casting solutions. After spreading the solutions on the glass plate, they were left to dry for at least 24 hours. Later, they were removed from the glass plate, washed with deionized water and dried at room temperature. These membranes were designated D31 and D11, which correspond to DMF/DEE ratios of 3/1 and 1/1, respectively. Table 1 shows the DMF/DEE weight ratios and solvent evaporation times of the membranes.

Table 1 – Solvent weight ratios and solvent evaporation times of the poly(ester urethane urea) membranes

Membranes	DMF/DEE weight ratio	Solvent evaporation time (min)
A31	3/1	1
A11	1/1	1
D31	3/1	-
D11	1/1	-

6.3 Structure characterization of the membranes by Scanning Electron Microscopy

Samples of the synthesized membranes were observed by Scanning Electron Microscopy (SEM). A31 and A11 were observed with a JSM-7001F FEG-SEM microscope (JEOL, Tokyo, Japan) and D31 and D11 with a Hitachi S-2400 SEM microscope (Hitachi, Tokyo, Japan). The samples were fractured after freezing in liquid nitrogen, mounted on a stub and sputter-coated with gold. Images of the top and bottom surfaces and of the cross-sections were obtained. The average thickness of the cross-sections and respective standard deviations were obtained by measurements of five regions in the cross section in SEM images using the software ImageJ version 1.50i (NIH ImageJ, USA) [69].

6.4 Gas permeation measurements

The gas permeation experiments on the poly(ester urethane urea) membranes were performed in the optimized setup, as shown in Figure 9, by the constant volume method. This method consists in determining the gas flux through the membrane by measuring the variation of pressure with time in the receiving chamber.

For a given measurement, the membrane is inserted in the cell and the setup is thermostated for at least 3 hours, until it stabilizes at a temperature of 37 ± 0.2 ºC. During this time, the membrane is degassed using the vacuum pump, with valves V1 and V5 closed and all the other valves opened. The volume of the receiving chamber can be chosen by manipulating valves V6 and V7. One gas (N_2, O_2, CO_2) is measured at a time by regulating the respective pressure reducing valve (PRV) to a feed pressures between 1.5 and 4 bar. To start the measurement, valves V2 and V3 are closed and the permeate pressure recording starts when V1 is opened. The feed pressure sensor is monitored to ensure that the feed pressure is constant. The pressure rise in the receiving chamber is recorded automatically at intervals of approximately 1.3 seconds and with a precision better than 10 Pa. After the measurement, V1 is closed and V2 and V3 are opened and the setup is degassed with the vacuum pump for at least 10 minutes before the next measurement. It was verified that this amount of time is enough to degass the membrane as no increase in pressure was observed after closing valve V3.

The average permeances, diffusion and solubility coefficients and respective standard deviations were calculated from the measurements of three excerpts of a membrane.

6.5 Gas solubility measurements by the barometric method

The gas solubility of one of the synthesized membranes, A31, for N_2, O_2 and CO_2 were measured independently by the barometric method, in order to compare the values obtained by the time lag method.

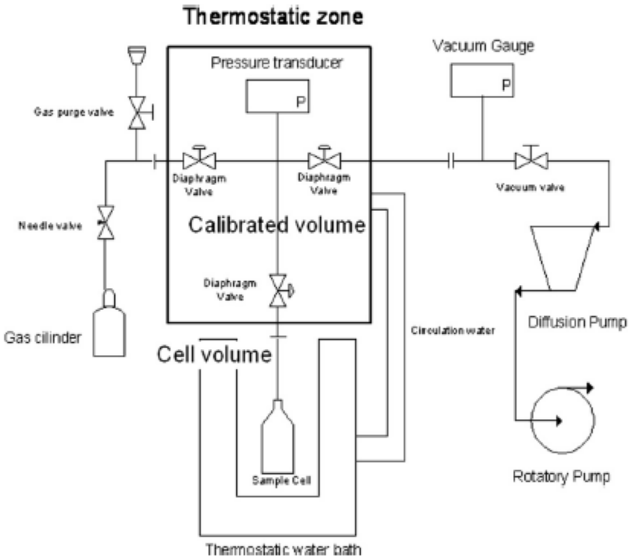

Figure 16 - Schematic representation of the volumetric apparatus for gas sorption experiments [70]

The gas sorption experiments were performed in a volumetric apparatus as shown in Figure 16, which method is described in [70]. The membrane was inserted in a cell, placed in the volumetric apparatus and put under high vacuum (Pfeiffer Vacuum, APR 266, vacuum below 10^{-2} Pa) for at least an hour. The apparatus has two chambers that are separated by a valve: one which volume was previously calibrated (chamber 1) and another where the cell is inserted along with the membrane sample (chamber 2), which volume is unknown. Volume calibration was carried out with helium. The measurements were performed at 37.5 ºC, using a water bath, and at pressures up to 4 bar. The gas is introduced in chamber 1 at a desired pressure, which value is registered. The gas is then expanded to chamber 2 by opening the valve and the pressure decay is monitored until it reaches a constant value (after 30-60 minutes). The final pressure value is registered and the sorbed gas is determined by mass balance. More gas is introduced into the system for the next measurement and this process is repeated until a complete isotherm is obtained.

To prevent contamination of the volumetric apparatus by the solvents used in the membrane synthesis, the membrane was previously put under vacuum in a Schlenk flask, at ambient temperature, for at least a week to ensure that no trace of solvent is left in the membrane.

The barometric method was attempted at the gas permeation setup for the solubility measurements of the membrane, which is described in Annex 11.2.

7 Results and Discussion

7.1 Structure characterization of the membranes by Scanning Electron Microscopy

Integral asymmetric poly(ester urethane urea) membranes A31 and A11 were synthesized with DMF/DEE weight ratios of 3/1 and 1/1, respectively, PUR/PCL weight ratio of 90/10, polymer/solvent ratio of 65/35 and solvent evaporation time of 1 minute.
Figure 17 shows the SEM images for the top and bottom surfaces and cross-sections of A31 and A11.

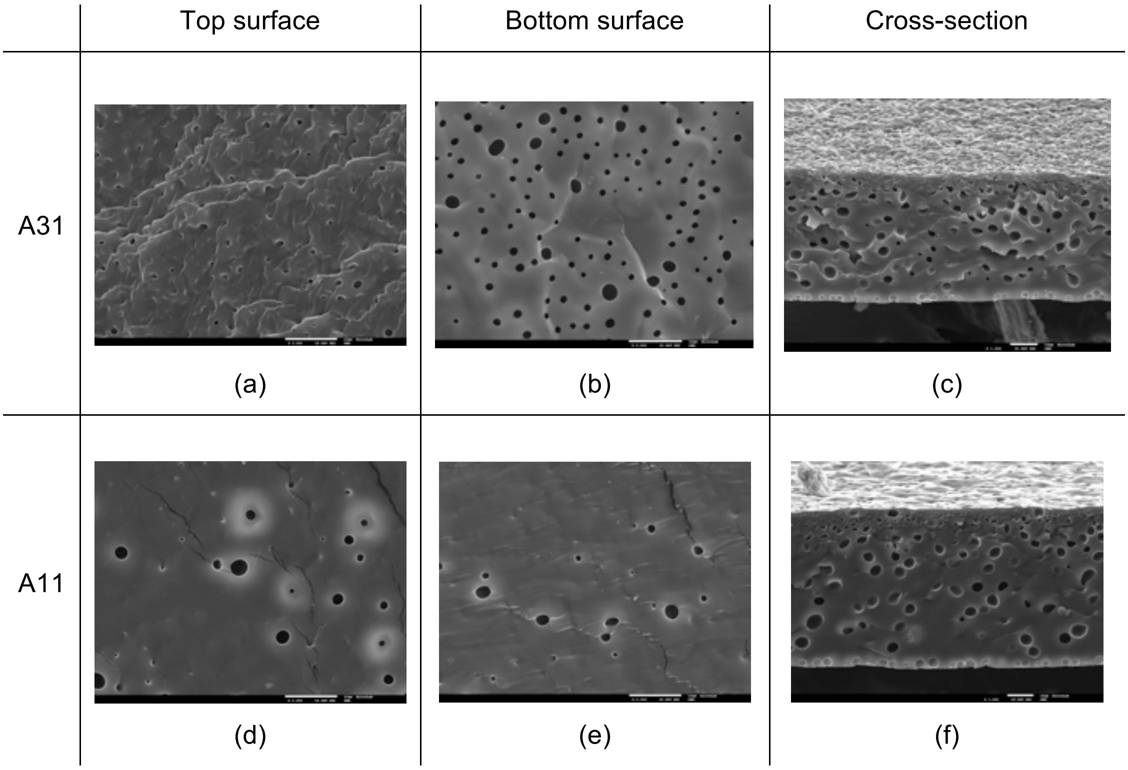

Figure 17 - SEM images of A31: (a) top surface, (b) bottom surface, (c) cross-section; A11: (d) top surface, (e) bottom surface, (f) cross-section

Observing the top surfaces (Figures 17a and 17d), A31 has more pore like features than A11. These pore like features will be referred to as pores in the rest of this work. In terms of size, the pores in A31 are all small and similar in size while A11 presents pores of different sizes and in some areas there are no visible pores. Regarding the bottom surfaces (Figures 17b and 17e), A31 has a porous surface, however, the pores are larger and lower in number compared to the top. The bottom surface of A11 is similar to its top surface. Relatively to the cross-sections (Figures 17c and 17f), a well defined dense layer on the top is not observed, probably because it is below the discrimination level of the technique, however, it can be seen that the pores on the top layer are smaller and larger in number compared to the lower layer. The average pore size and polymer surface area coverage were determined by the

ImageJ software, as shown in Table 2. The average pore size results from the ratio between the sum of the areas of the pores and the number of pores.

Table 2 - Average pore size and polymer surface area coverage of A31 and A11

Membrane		Average pore size (µm^2)	Polymer surface area coverage (%)
A31	top	0.15	99
	bottom	1.31	94
A11	top	1.74	98
	bottom	1.51	99

Nonporous symmetric poly(ester urethane urea) membranes D31 and D11 were synthesized with DMF/DEE weight ratios of 3/1 and 1/1, respectively, PUR/PCL weight ratio of 90/10 and polymer/solvent ratio of 65/35.

Figure 18 shows the SEM images for the top and bottom surfaces and cross-sections of D31 and D11.

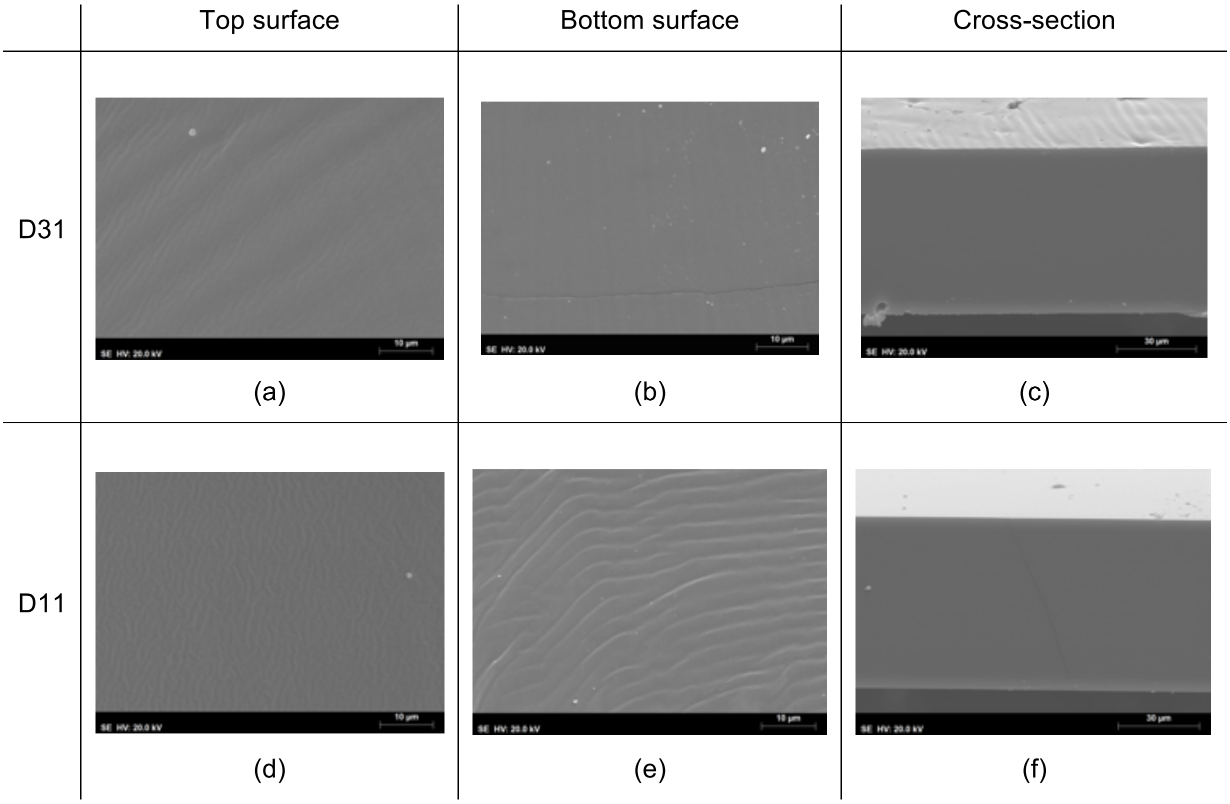

Figure 18 - SEM images of D31: (a) top surface, (b) bottom surface, (c) cross-section; D11: (d) top surface, (e) bottom surface, (f) cross-section

From the SEM images in Figure 18, it can be seen that D31 and D11 are completely dense.

The total thickness of the membranes were measured from the cross-sections SEM images using the software ImageJ. The average thickness and respective standard deviations (σ) are represented in Table 3.

Table 3 - Average thickness and respective standard deviation of the membranes

Membrane	Thickness, l (μm)	σ (μm)
A31	46	0.9
A11	61	0.5
D31	63	0.3
D11	64	0.1

7.2 Gas permeation measurements

N_2, O_2 and CO_2 gas permeation experiments were performed on the poly(ester urethane urea) membranes by the constant volume method, where the pressure rise in the receiving chamber, initially in vacuum, was recorded online, at a temperature of 37 ºC. Figure 19 shows the permeation curves for the three gases, obtained for the A31 membrane. Similar permeation curves were obtained for the other membranes.

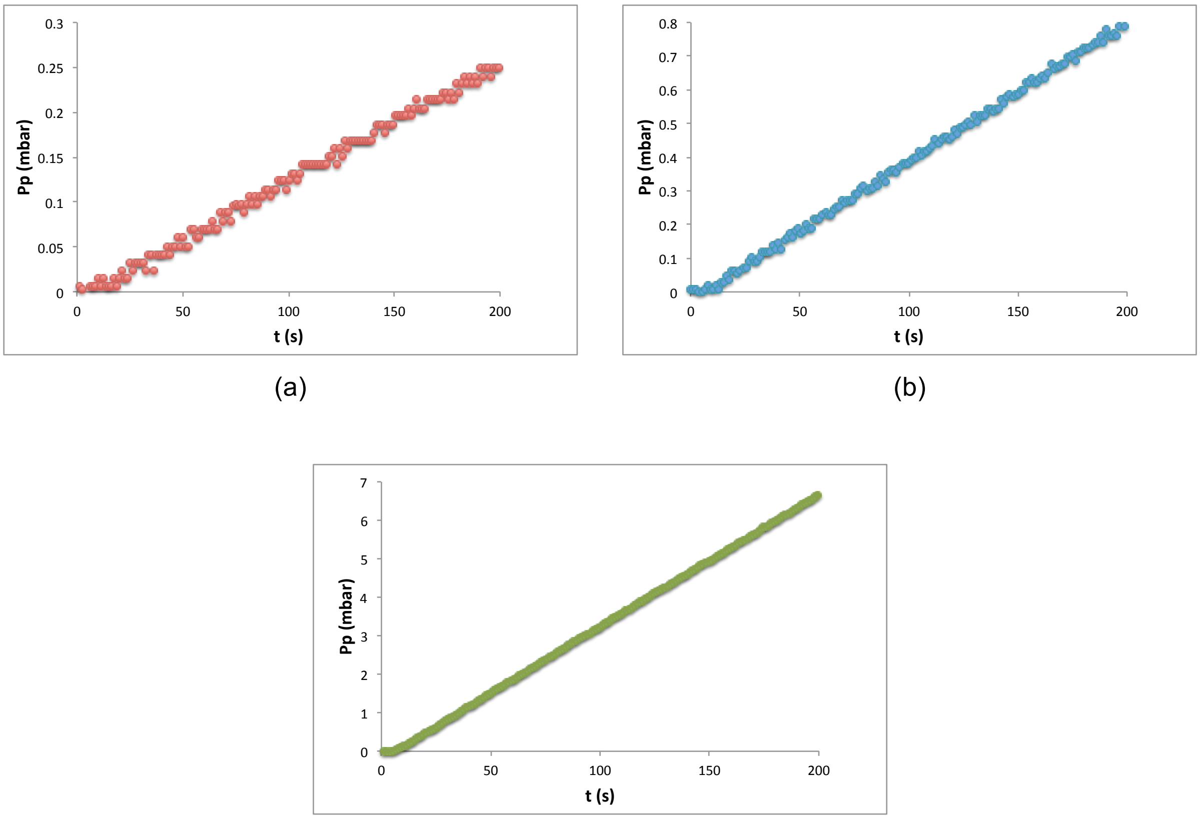

(a)

(b)

(c)

Figure 19 – Permeate pressure vs time for A31 membrane with (a) N_2 at P_f = 2.3 bar, (b) O_2 at P_f = 2.4 bar and (c) CO_2 at P_f = 2.2 bar

In Figure 19, a transient state and a steady state can be distinguished for all three gases. At similar feed pressures, after 200 seconds the permeate pressure increased 0.25, 0.80 and 7.0 mbar for N_2, O_2 and CO_2, respectively.

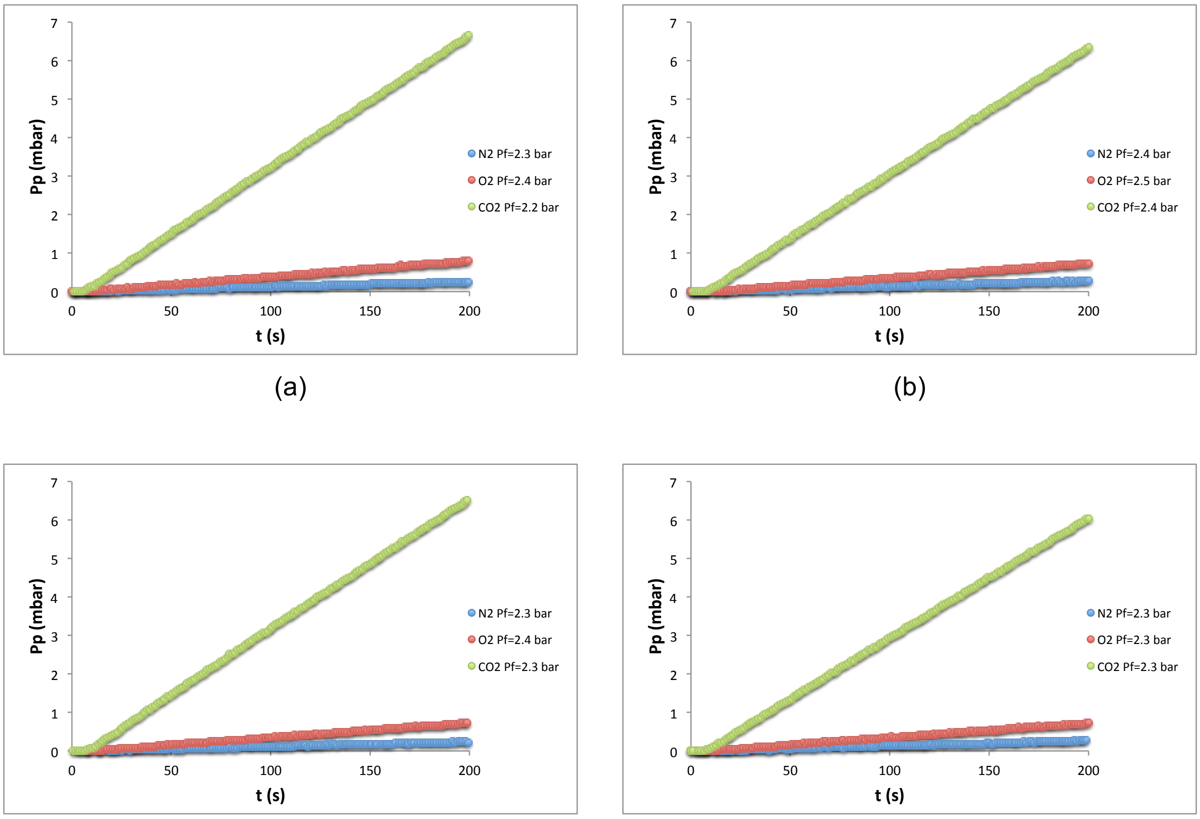

(a) (b)

(c) (d)

Figure 20 – N_2, O_2 and CO_2 permeate pressures vs time for membranes (a) A31, (b) A11, (c) D31 and (d) D11

Figure 20 shows that, at similar feed pressures, the steady state slope increases in the order of N_2, O_2 and CO_2 for all membranes.

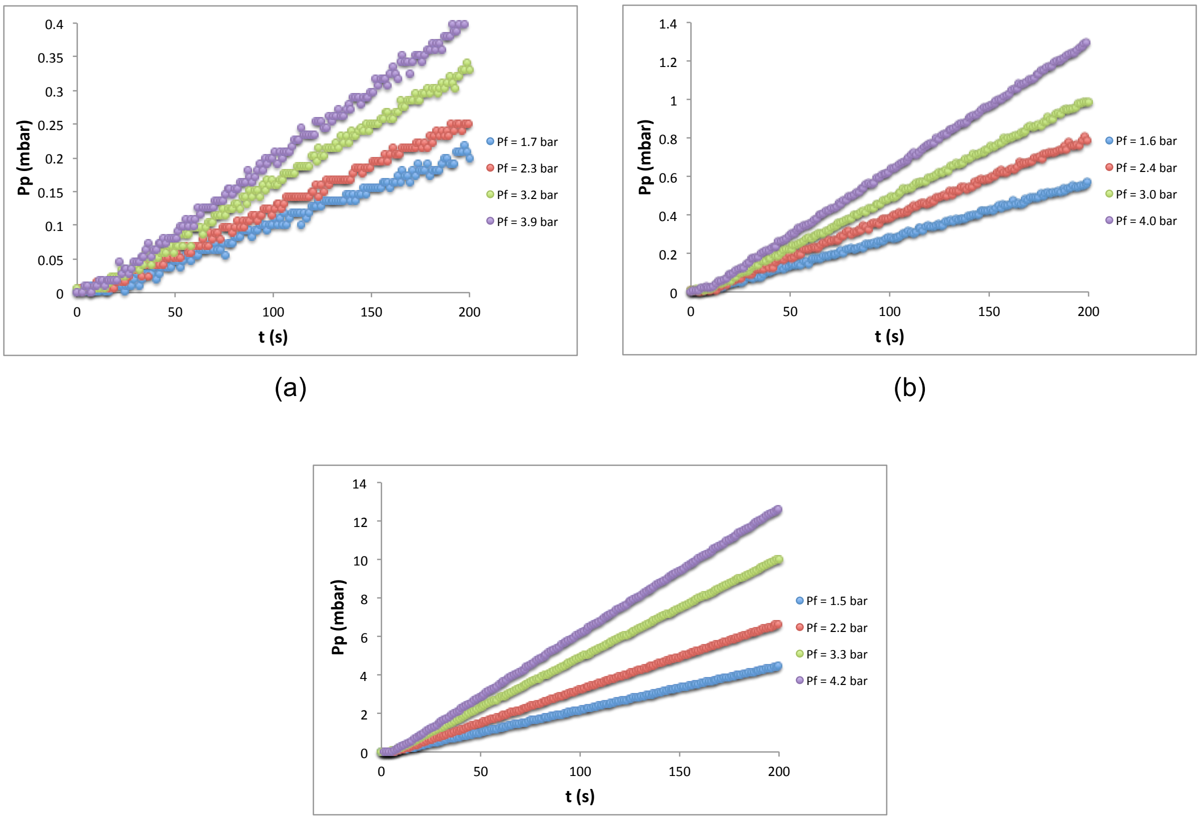

(a) (b)

(c)

Figure 21 – Permeate pressure vs time for A31 membrane with (a) N_2, (b) O_2 and (c) CO_2 at different feed pressures

Figure 21 shows the N_2, O_2 and CO_2 permeation curves for A31 membrane at different feed pressures. From each steady state slope, $\frac{dp_p}{dt}$, a volumetric flux, J, can be obtained.

In order to determine the volumetric flux some calculations are required as shown below. First, the steady state slope, $\frac{dp_p}{dt}$, is converted into molar flow, $\frac{dn}{dt}$, by using the Ideal Gas Law:

$$\frac{dn}{dt} = \frac{dp_p}{dt}\frac{V_s}{RT} \tag{25}$$

where V_s is the volume of the receiving chamber and T is the absolute temperature at which the experiments are performed. Then, the molar flow is converted into volumetric flow, $\frac{dV}{dt}$, in STP conditions:

$$\frac{dV}{dt} = \frac{dn}{dt}\frac{RT_{STP}}{P_{STP}} \tag{26}$$

where T_{STP} and P_{STP} are the temperature and pressure in STP conditions, which are 273.15 K and 1 atm. Substituting Equation 25 in Equation 26, the following expression is obtained:

$$\frac{dV}{dt} = \frac{dp_p}{dt}\frac{V_s T_{STP}}{T P_{STP}} \tag{27}$$

The volumetric flux is then obtained by dividing the volumetric flow by the effective membrane area, A:

$$J = \frac{dV}{Adt} \tag{28}$$

Plots of the volumetric fluxes (J) vs the transmembrane pressure (TMP) were obtained for all membranes, as shown in Figure 22. TMP is the difference between the feed pressure and the initial permeate pressure ($TMP = p_f - p_p(t = 0)$), which is approximately 0 mbar.

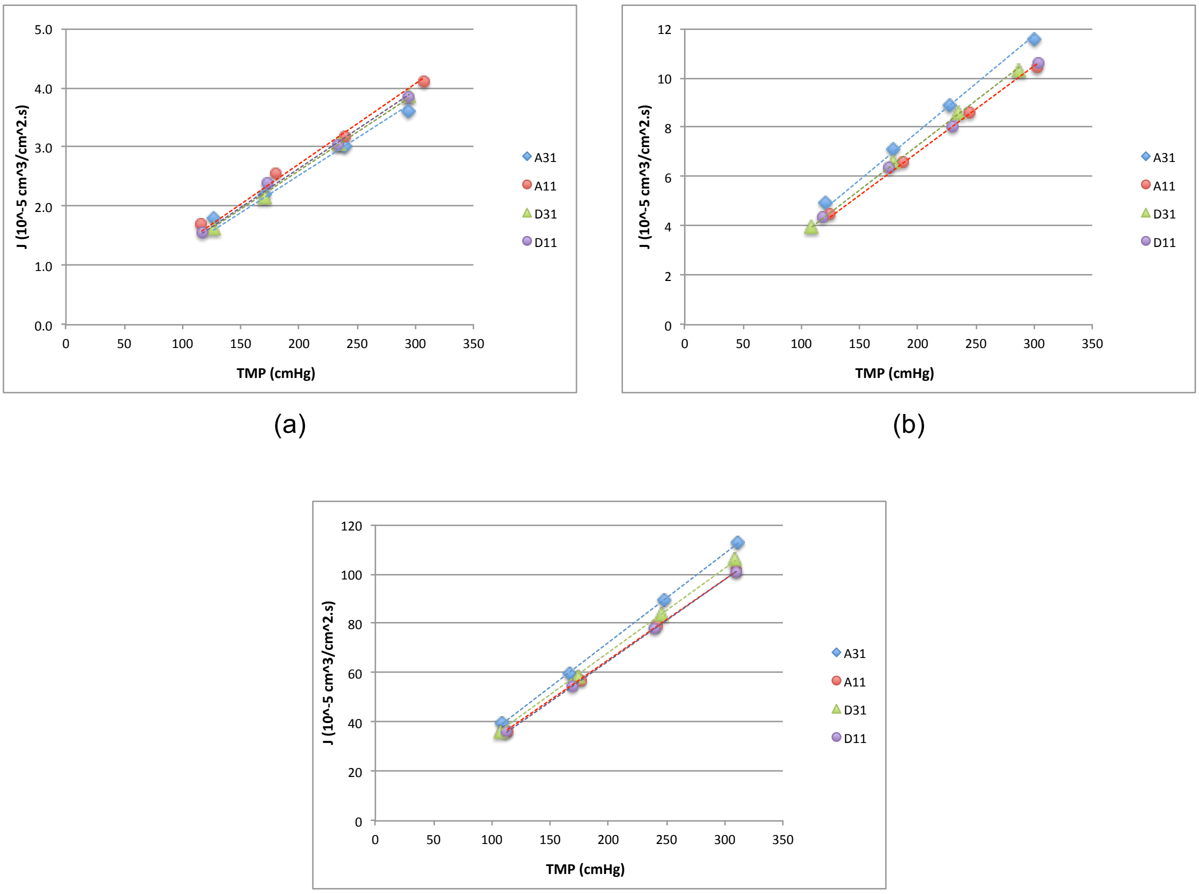

(a) (b)

(c)

Figure 22 – (a) N_2, (b) O_2 and (c) CO_2 volumetric fluxes vs the transmembrane pressure for membranes A31, A11, D31 and D11

As can be seen in Figure 22, similar volumetric fluxes were obtained for all membranes. The volumetric fluxes increase in the order of N_2, O_2 and CO_2.

Table 4 and Figure 23 shows the extrapolated N_2, O_2 and CO_2 volumetric fluxes obtained for membranes A31, A11, D31 and D11 at a feed pressure of 1 bar.

Table 4 - N_2, O_2 and CO_2 volumetric fluxes for membranes A31, A11, D31 and D11 at a feed pressure of 1 bar

Membrane	J_{N_2} (10^{-5} cm^3/cm^2.s)	J_{O_2} (10^{-5} cm^3/cm^2.s)	J_{CO_2} (10^{-5} cm^3/cm^2.s)
A31	0.96 ± 0.14	2.6 ± 0.32	25.8 ± 2.6
A11	0.95 ± 0.01	2.6 ± 0.03	25.1 ± 0.6
D31	0.96 ± 0.04	2.6 ± 0.08	25.5 ± 0.8
D11	0.91 ± 0.04	2.5 ± 0.07	24.0 ± 0.9

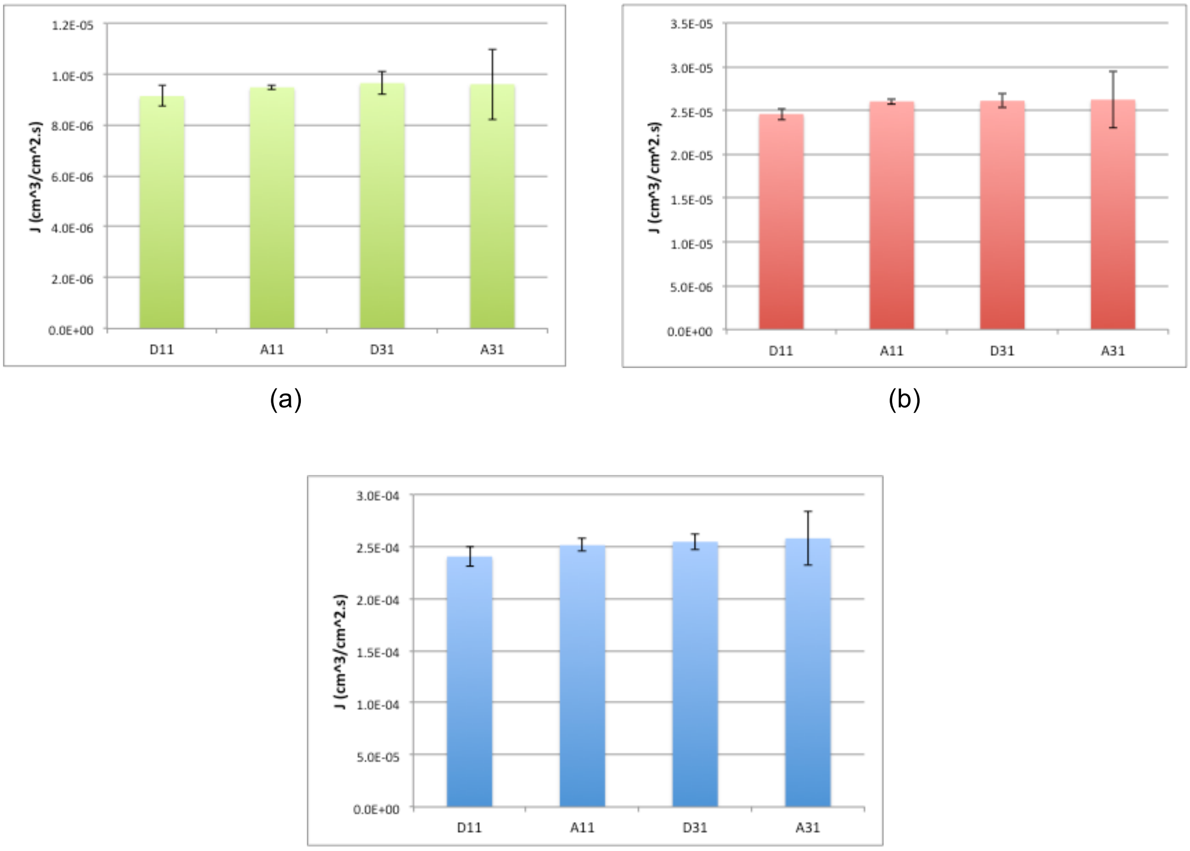

(a)

(b)

(c)

Figure 23 – (a) N_2, (b) O_2 and (c) CO_2 volumetric fluxes obtained for membranes A31, A11, D31 and D11

The permeances, $Perm$, were obtained from the slopes of the volumetric flux vs TMP plots:

$$Perm = \frac{dJ}{d(TMP)} \left[\frac{cm^3(STP)}{cm^2\ s\ cmHg}\right] \tag{29}$$

The obtained thickness and average N_2, O_2 and CO_2 permeances with respective standard deviations for each membrane are shown in Table 5.

Table 5 – Thickness and average N_2, O_2 and CO_2 permeances for membranes A31, A11, D31 and D11

Membrane	Thickness, $\boldsymbol{l}$ (μm)	$\boldsymbol{Perm_{N_2}}$ (10^{-6} cm^3/cm^2.s.cmHg)	$\boldsymbol{Perm_{O_2}}$ (10^{-6} cm^3/cm^2.s.cmHg)	$\boldsymbol{Perm_{CO_2}}$ (10^{-6} cm^3/cm^2.s.cmHg)
A31	46	0.13 ± 0.02	0.35 ± 0.04	3.4 ± 0.3
A11	61	0.12 ± 0.00	0.34 ± 0.00	3.3 ± 0.1
D31	63	0.13 ± 0.01	0.34 ± 0.01	3.4 ± 0.1
D11	64	0.12 ± 0.01	0.32 ± 0.01	3.2 ± 0.1

The average values of permeances obtained for each gas is similar for all membranes. The CO_2 permeances are approximately 30 times and 10 times higher than the N_2 and O_2 permeances, respectively. Table 6 shows the ideal selectivities obtained for the membranes.

Table 6 – Ideal selectivities obtained for membranes A31, A11, D31 and D11

Membrane	$\propto_{\boldsymbol{O_2/N_2}}$	$\propto_{\boldsymbol{CO_2/O_2}}$	$\propto_{\boldsymbol{CO_2/N_2}}$
A31	2.7	9.8	26.9
A11	2.7	9.7	26.5
D31	2.7	9.8	26.4
D11	2.7	9.8	26.3

The permeances of the nonporous symmetric membranes were converted to permeability coefficients (P) in Barrer units by the expression below:

$$P = Perm \times l \times 10^{10}\ [Barrer] \tag{30}$$

Table 7 shows the average permeability coefficients of all three gases for the nonporous symmetric membranes and the respective standard deviations.

Table 7 – N_2, O_2 and CO_2 permeability coefficients obtained for membranes D31 and D11

Membrane	$\boldsymbol{P_{N_2}}$ (Barrer)	$\boldsymbol{P_{O_2}}$ (Barrer)	$\boldsymbol{P_{CO_2}}$ (Barrer)
D31	8 ± 0	21 ± 0	208 ± 6
D11	8 ± 0	21 ± 0	202 ± 4

Faria *et al*. [57] have reported P_{CO_2} values between 113 and 337 Barrer and P_{O_2} values between 10 and 11 Barrer for nonporous symmetric membranes containing 0 to 15 weight % PCL. For 10 weight % of PCL, the values of P_{CO_2} and P_{O_2} were 337 Barrer and 11 Barrer, respectively, which is higher than the P_{CO_2} (208 and 202 Barrer) and lower than the P_{O_2} (21 Barrer) obtained for membranes D31 and D11.

In comparison to other membranes of current MBOs, the obtained P_{CO_2} values are higher than the values of PP (9 Barrer) and PMP (90 Barrer) membranes. The obtained P_{O_2} values are in between the values of PP (2 Barrer) and PMP (30 Barrer) membranes [71].

A Membrane Blood Oxygenator (MBO) is required to deliver about 250 cm^3(STP)/min of O_2 and remove about 200 cm^3(STP)/min of CO_2 [8]. The surface area of membrane demanded to meet these requirements was estimated from the obtained volumetric fluxes at a feed pressure of 1 bar, as presented in Table 8.

Table 8 - O_2 and CO_2 volumetric fluxes for membranes A31, A11, D31 and D11 and estimated membrane surface area for MBOs

Membrane	J_{O_2} (10^{-5} $cm^3/cm^2.s$)	Membrane surface area (m^2)	J_{CO_2} (10^{-5} $cm^3/cm^2.s$)	Membrane surface area (m^2)
A31	2.6	15.9	25.8	1.3
A11	2.6	16.0	25.1	1.3
D31	2.6	16.0	25.5	1.3
D11	2.5	16.9	24.0	1.4

Due to high CO_2 permeation properties, the MBOs would require a total membrane surface area of approximately 1.3 m^2, which is lower than the membrane surface area of current commercial MBOs, which is approximately 2 m^2 [72]. As for O_2, because of its low permeation properties it would require a total membrane surface area of about 16 m^2 which is inconvenient, as it is an order of magnitude higher than the average membrane surface area of commercial MBOs. However, it should be reminded that these membranes have better hemocompatibility [54], which might make it acceptable to have a MBO with a larger surface area.

7.3 Determination of the diffusion and solubility coefficients

The diffusion and solubility coefficients of the poly(ester urethane urea) membranes were determined by the time lag method. From each permeation curve, a time lag was obtained from the intersection of the steady state asymptote with the time axis, as shown in Figure 24.

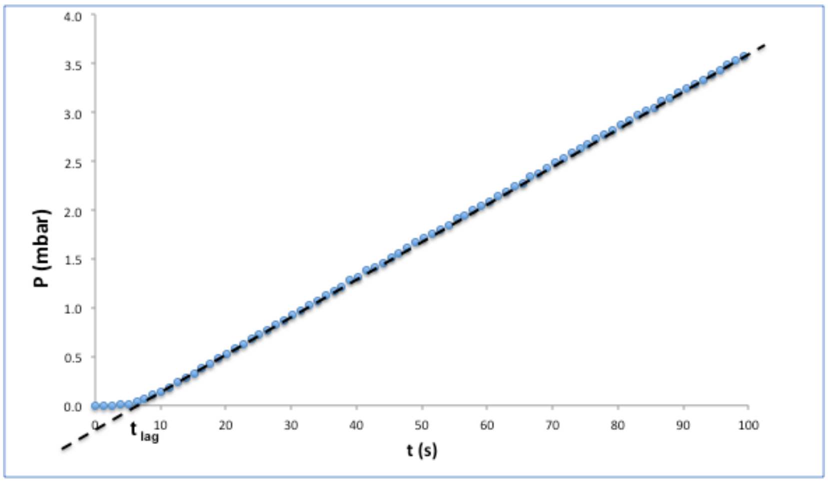

Figure 24 - CO_2 permeate pressure vs time for the A31 membrane at a feed pressure of 2.3 bar

The diffusion coefficients were calculated using Equation 17 in section 4.2 and the obtained values are shown in Table 9 and Figure 25, along with the average time lags.

Table 9 – N_2, O_2 and CO_2 average time lags, diffusion coefficients and respective standard deviations obtained for membranes A31, A11, D31 and D11

Membrane	$t_{lag_{N_2}}$ (s)	D_{N_2} (10^{-7} cm^2/s)	$t_{lag_{O_2}}$ (s)	D_{O_2} (10^{-7} cm^2/s)	$t_{lag_{CO_2}}$ (s)	D_{CO_2} (10^{-7} cm^2/s)
A31	5.1	7.1 ± 0.6	4.8	7.4 ± 1.4	4.8	7.5 ± 1.4
A11	4.7	12.9 ± 3.2	6.9	8.9 ± 1.6	5.4	11.3 ± 1.9
D31	6.9	9.5 ± 0.9	6.2	10.7 ± 0.7	8.8	12.2 ± 0.5
D11	5.2	13.0 ± 4.0	6.2	11.0 ± 0.5	5.7	11.9 ± 0.6

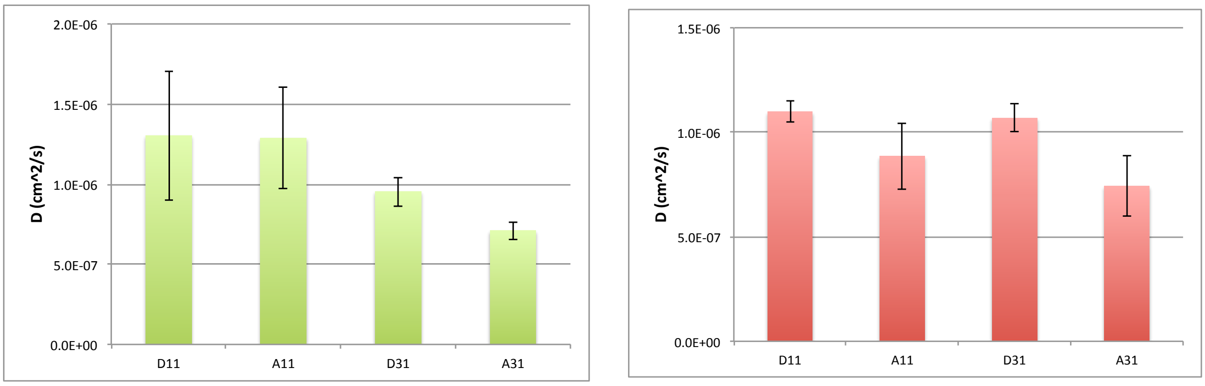

(a) (b)

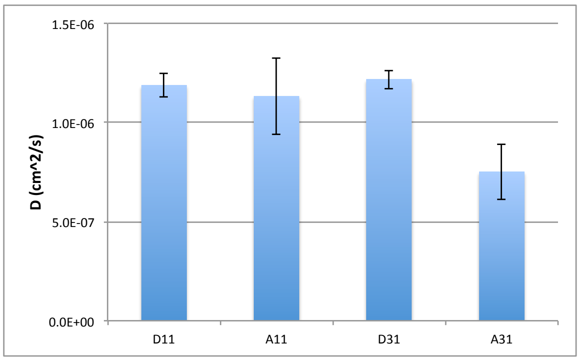

(c)

Figure 25 – (a) N_2, (b) O_2 and (c) CO_2 diffusion coefficients and respective standard deviations obtained for membranes A31, A11, D31 and D11

An ANOVA test was executed to compare the obtained average values of the diffusion coefficients between the membranes. This test is a way to compare means of different groups to see if the differences between them are statistically significant. The test showed that there is a significant difference between them for a confidence level of 95%.

The solubility coefficients were determined by dividing the permeability coefficients $(Perm \times l)$ by the diffusion coefficients (Equation 1).

Table 10 – N_2, O_2 and CO_2 average solubility coefficients and respective standard deviations obtained for membranes A31, A11, D31 and D11

Membrane	S_{N_2} (10^{-2} cm^3/cm^{3}cmHg)	S_{O_2} (10^{-2} cm^3/cm^{3}cmHg)	S_{CO_2} (10^{-2} cm^3/cm^{3}cmHg)
A31	0.08 ± 0.01	0.25 ± 0.05	2.2 ± 0.2
A11	0.07 ± 0.02	0.25 ± 0.04	1.8 ± 0.3
D31	0.08 ± 0.01	0.22 ± 0.01	1.7 ± 0.1
D11	0.07 ± 0.01	0.20 ± 0.00	1.7 ± 0.1

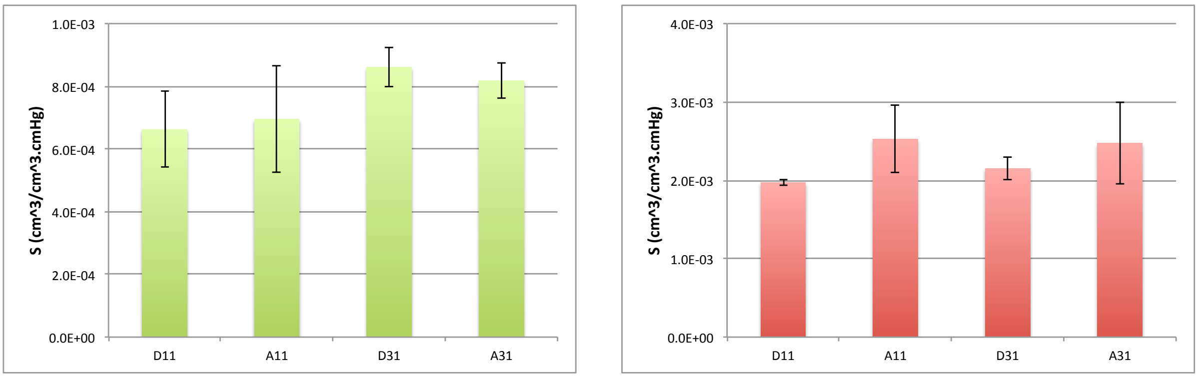

(a) (b)

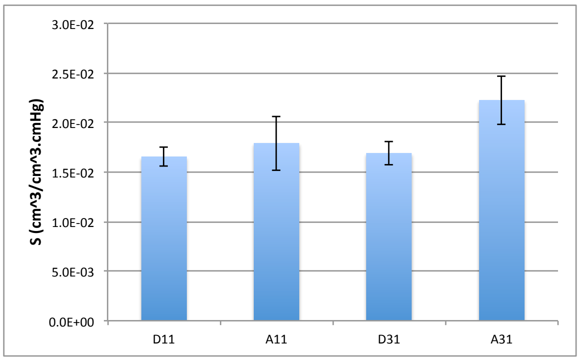

(c)

Figure 26 – (a) N_2, (b) O_2 and (c) CO_2 solubility coefficients and respective standard deviations obtained for membranes A31, A11, D31 and D11

Results from the ANOVA test showed that there is no significant difference between the mean values of N_2 solubilities for a confidence level of 95%, however, the opposite was observed for the mean values of O_2 and CO_2 solubilities.

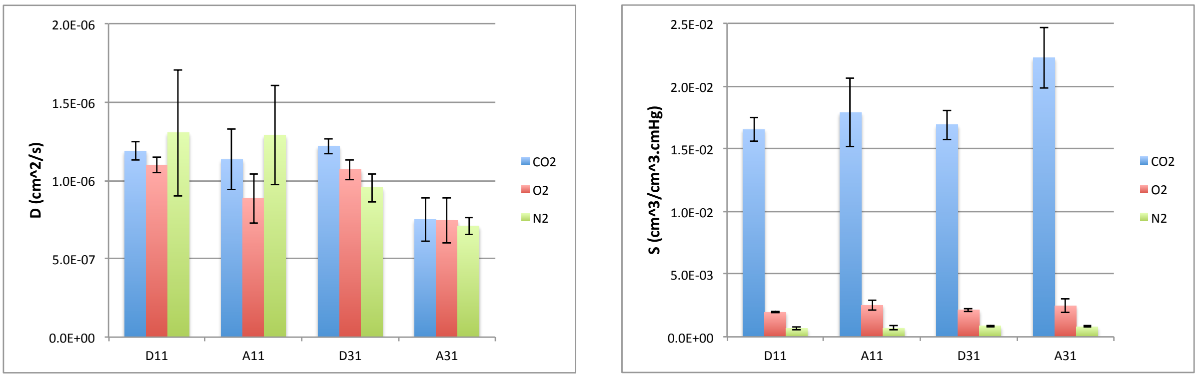

(a) (b)

Figure 27 – (a) Diffusion coefficients and (b) solubility coefficients and respective standard deviations obtained for N_2, O_2 and CO_2 for membranes A31, A11, D31 and D11

Table 11 – N_2, O_2 and CO_2 kinetic diameters and boiling points [73]

Molecule	kinetic diameter (Å)	boiling point (ºC)
CO_2	3.30	-78.5
O_2	3.46	-183
N_2	3.64	-196

As it can be seen in Figure 27, the biggest difference is in the solubility coefficients of the gases in these poly(ester urethane urea) membranes, while not much difference is seen in the diffusion coefficients. Therefore, the solubility is the main contributing factor for the observed difference in permeabilities of the three gases.

Regarding the solubility coefficient, it has been proposed that it is dependant on the gas boiling point or critical temperature [11]. As shown in Table 11, CO_2 has the highest boiling point, which explains its high solubility in the membrane. The boiling points increase in the order of N_2, O_2 and CO_2 and this same trend is observed in the obtained solubility coefficients as shown in Figure 27.

As for the diffusion coefficient, it is known to be dependant on the size of the gas molecule: as the kinetic diameter of the gas molecule increases the diffusion coefficient decreases [11]. From the kinetic diameters shown in Table 11, it would be expected that the diffusion coefficient increases in the order of N_2, O_2 and CO_2. This tendency is observed for membranes D31 and A31 but not for D11 and A11, as shown in Figure 27.

Faria *et al*. [57] have obtained D_{CO_2} and S_{CO_2} values of 8.15 x 10^{-7} cm^2/s and 4.14 x 10^{-2} cm^3/cm^3cmHg, respectively, for membranes containing 10 weight % of PCL, which is in the same order of magnitude as the values obtained in this study.

Another method alternative to the time lag for the determination of the diffusion coefficient is the early approximation method, which is presented in Annex 11.3.

7.4 Gas solubility measurements by the barometric method

The N_2, O_2 and CO_2 solubilities in membrane A31 were measured by the barometric method in order to compare them to the results obtained from the time lag method. A sorption isotherm was obtained for each gas up to a pressure of 4 bar, as shown in Figure 28.

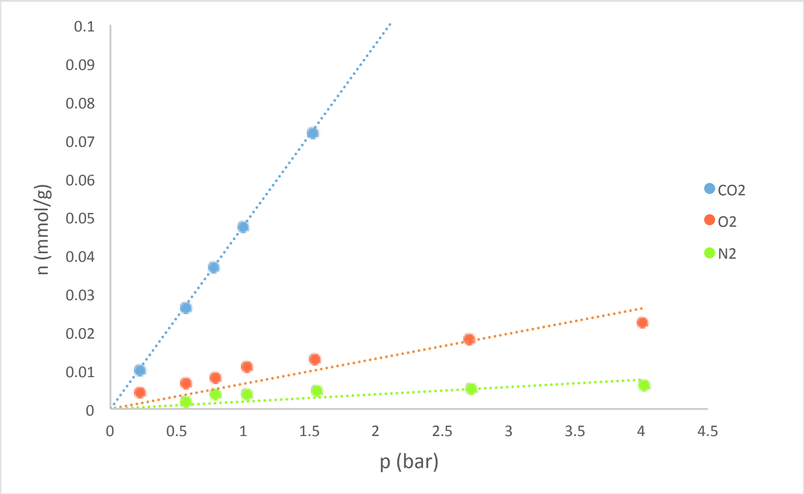

Figure 28 – N_2, O_2 and CO_2 sorption isotherms obtained for membrane A31

It can be seen in Figure 28 that the O_2 and N_2 isotherms show some deviation to the fitted line, possibly because these gases are sorbed by the membrane in very low quantities, which are at the limit of application of the used apparatus.

The solubility was obtained from the slope of each isotherm, assuming the validity of Henry´s Law, and is represented as a horizontal line in Figure 29.

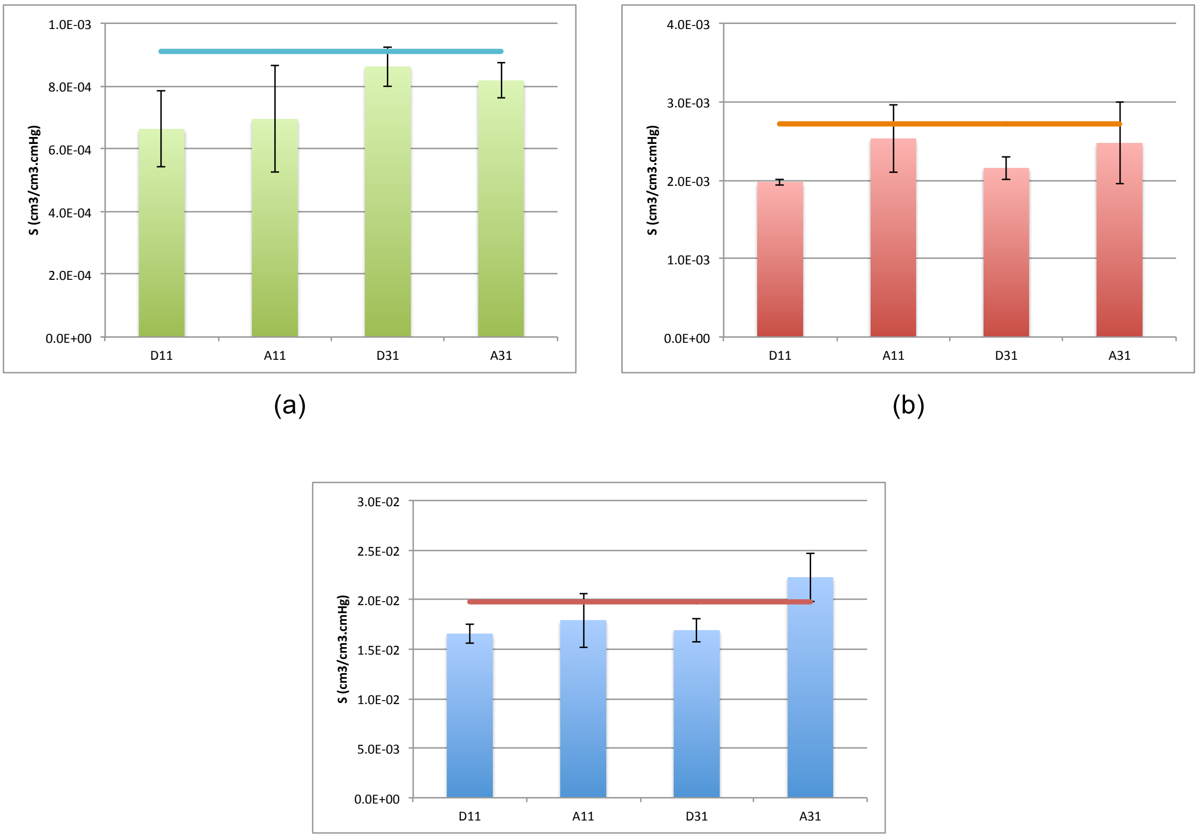

(a)

(b)

(c)

Figure 29 – (a) N_2, (b) O_2 and (c) CO_2 solubility coefficients obtained for membranes A31, A11, D31 and D11 by the time lag method in comparison with the solubility coefficient obtained by solubility measurement of A31 (horizontal line)

As shown in Figure 29, the solubilities obtained by the barometric method agree with the results obtained by the time lag method, within the experimental uncertainty. This validates the measurements obtained in the current gas permeation setup.

8 Conclusions

The gas permeation setup was optimized by increasing the volume of the receiving chamber and performing vacuum to the setup before the measurements in order to obtain more precise results. A non-negligible resistance to gas transport was observed during measurements as a consequence of the Knudsen flow, which affected the results of permeances and time lags. The effect of the resistance ceased after substituting the big cylinder with volume of 394.9 ± 1.5 cm^3 for a smaller one with volume of 167.2 ± 0.2 cm^3 and placing the pressure transmitter at the end of the main tube. Overall, the current gas permeation setup, with a receiving chamber with a total volume of 193.3 ± 0.3 cm^3, is capable of measuring, at constant temperature, the permeate pressure rise online in the receiving chamber at intervals of 1.3 seconds and with a precision better than 10 Pa, providing highly reproducible results of permeances. Additionally, a transient state was observed for N_2, O_2 and CO_2, which permitted the application of the time lag method for the determination of the diffusion and solubility coefficients.

Integral asymmetric poly(ester urethane urea) membranes A31 and A11 were synthesized by a modified version of the phase inversion technique with DMF/DEE weight ratios of 3/1 and 1/1, respectively, PUR/PCL weight ratio of 90/10, polymer/solvent ratio of 65/35 and solvent evaporation time of 1 minute. SEM images revealed that the asymmetry is more noticeable in the membrane A31 than A11, as the difference in the average pore size between the top and bottom layers is bigger and the polymer surface area coverage is smaller in the bottom compared to the top. However, a well defined dense layer on the top is not observed, probably because it is below the discrimination level of the technique. The measured total thickness for A31 and A11 were 46 μm and 61 μm, respectively.

Nonporous symmetric poly(ester urethane urea) membranes D31 and D11 were synthesized by the solvent evaporation technique with DMF/DEE weight ratios of 3/1 and 1/1, respectively, PUR/PCL weight ratio of 90/10 and polymer/solvent ratio of 65/35. SEM images showed them to be completely dense. The measured total thickness for D31 and D11 were 63 μm and 64 μm, respectively.

Similar permeances were obtained for the integral asymmetric and nonporous symmetric membranes: 0.12-0.13x10^{-6} cm^3/cm^2scmHg for N_2, 0.32-0.35x10^{-6} cm^3/cm^2scmHg for O_2 and 3.2-3.4x10^{-6} cm^3/cm^2scmHg for CO_2. The permeability coefficients obtained for the symmetric membranes were: 8 Barrer for N_2, 21 Barrer for O_2 and 202 Barrer (D11) and 208 Barrer (D31) for CO_2.

The membranes showed great CO_2 permeation properties, resulting in an estimated eventual requirement of less membrane surface area than the one of current commercial MBOs, which is approximately 2 m^2. However, it showed low O_2 permeation properties, which would require a total membrane surface area of about 16 m^2. Although it may be inconvenient, these membranes have better hemocompatibility which may compensate for its larger area.

The diffusion coefficients obtained by the time lag method were: 7.1-13.0x10^{-7} cm^2/s for N_2, 7.4-11.0x10^{-7} cm^2/s for O_2 and 7.5-12.2x10^{-7} cm^2/s for CO_2. The solubility coefficients obtained were: 0.07-0.08x10^{-2} cm^3/cm^3cmHg for N_2, 0.20-0.25x10^{-2} cm^3/cm^3cmHg for O_2 and 1.7-2.2x10^{-2} cm^3/cm^3cmHg

for CO_2. From these results it can be concluded that the solubility is the main contributing factor for the difference in permeabilities of the three gases. Therefore, gas permeation properties, particularly of O_2, may be improved by enhancing the solubility coefficients.

The solubilities obtained by the barometric method were 0.09×10^{-2} $cm^3/cm^3.cmHg$ for N_2, 0.27×10^{-2} $cm^3/cm^3.cmHg$ for O_2 and 1.98×10^{-2} $cm^3/cm^3.cmHg$ for CO_2, which are in agreement with the values obtained by the time lag method, within the experimental uncertainty, which validates the measurements obtained in the current gas permeation setup.

9 Perspectives for future work

The current gas permeation setup may be further improved by following the suggestions presented in Chapter 5 as guidelines, such as using tubes of larger diameter and using cylinders of similar volume.

Improvements in O_2 permeation properties of the poly(ester urethane urea) membranes are still needed, specifically by enhancing the solubility coefficients and this may be performed, for example, by varying the ratios of the reagents in the casting solutions.

Gas permeability of membranes containing 15% PCL may be measured in the current gas permeation setup as it was reported to have better hemocompatibility than membranes containing 10% PCL [54]. Because of this characteristic, it may find its use in other applications in the biomedical field.

Permeabilities to other gases of poly(ester urethane urea) membranes containing PCL as a second soft segment should be measured as they may be useful in other gas separation applications.

10 Bibliography

[1] Stuart Fox, *Human Physiology*, 14th ed.: McGraw-Hill Education, 2015.

[2] WHO - World Health Organization. (2018) The top 10 causes of death. [Online]. http://www.who.int/en/news-room/fact-sheets/detail/the-top-10-causes-of-death (Consulted in August 2018)

[3] G. P. Gravlee, R. F. Davis, J. W. Hammon, and B. D. Kussman, *Cardiopulmonary Bypass and Mechanical Support - Principles and practice*, 4th ed.: Wolters Kluwer, 2015.

[4] A. M. Gaffney, S. M. Wildhirt, M. J. Griffin, G. M. Annich, and M. W. Radomski, "Extracorporeal life support," *BMJ*, vol. 431, pp. 982-986, 2010.

[5] T. Yeager and S. Roy, "Evolution of Gas Permeable Membranes for Extracorporeal Membrane Oxygenation," *Artificial Organs*, vol. 41, no. 8, pp. 700-709, 2017.

[6] S. Slack, DO, and H. Stoecklein. (2017, Dec.) ECMO & ECPR. [Online]. https://www.jems.com/articles/supplements/special-topics/ems-state-of-the-science/ecmo-ecpr.html (Consulted in August 2018)

[7] JH Jr Gibbon, "The application of a mechanical heart and lung apparatus to cardiac surgery," *Minn Med*, vol. 37, no. 171, 1954.

[8] D. F. Stamatialis et al., "Medical applications of membranes: Drug delivery, artificial organs and tissue engineering," *Journal of Membrane Science*, vol. 308, pp. 1-34, 2008.

[9] GH Jr Clowes and AL Hopkins, "Further studies with plastic films and their use in oxygenating blood," *Trans Am Soc Artif Intern Organs*, vol. 1, pp. 23-24, 1955.

[10] A. F. Ismail, K. C. Khulbe, and T. Matsuura, *Gas separation Membranes - Polymeric and inorganic*, 1st ed.: Springer International Publishing, 2015.

[11] Richard W. Baker and Bee Ting Low, "Gas Separation Membrane Materials: A Perspective," *Macromolecules*, vol. 47, pp. 6999-7013, 2014.

[12] P. Bernardo, E. Drioli, and G. Golemme, "Membrane Gas Separation: A Review/State of the Art," *Ind. Eng. Chem. Res*, vol. 48, pp. 4638-4663, 2009.

[13] K. V. Peinemann, "Membrane Based Gas Separation - past, presence and future," *Membrane*, vol. 31, pp. 165-169, 2006.

[14] P. M. Budd and N. B. McKeown, "Highly permeable polymers for gas separation membranes," *Polymer Chemistry*, vol. 1, pp. 63-68, 2010.

[15] B. D. Bhide, A. Voskericyan, and S. A. Stern, "Hybrid processes for the removal of acid gases from natural gas," *Journal of Membrane Science*, vol. 140, p. 27, 1998.

[16] L. S. White, T. A. Blinka, H. A. Kloczewski, and I. F. Wang, "Properties of a polyimide gas separation membrane in natural gas," *Journal of Membrane Science*, vol. 103, pp. 73-82, 1995.

[17] C. Ma and W. J. Koros, "High-performance ester-crosslinked hollow fiber membranes for natural gas separations," *Journal of Membrane Science*, vol. 428, pp. 251-259, 2013.

[18] H. An et al., "Bromination/Debromination-Induced Thermal Crosslinking of 6FDA-Durene for Aggressive Gas Separations," *Journal of Membrane Science*, vol. 545, pp. 358-366, 2018.

[19] N. Du, M. M. Dal-Cin, G. P. Robertson, and M. D. Guiver, "Decarboxylation-Induced Cross-Linking of

Polymers of Intrinsic Microporosity (PIMs) for Membrane Gas Separation," *Macromolecules*, vol. 45, pp. 5134-5139, 2012.

[20] B. Molki, W. M. Aframehr, R. Bagheri, and J. Salimi, "Mixed matrix membranes of polyurethane with nickel oxide nanoparticles for CO2 gas separation," *Journal of Membrane Science*, vol. 549, pp. 588-601, 2018.

[21] H. Zhao et al., "High performance post-modified polymers of intrinsic microporosity (PIM-1) membranes based on multivalent metal ions for gas separation," *Journal of Membrane Science*, vol. 514, pp. 305-312, 2016.

[22] Z. Zhang et al., "Silver-doped strontium niobium cobaltite as a new perovskite-type ceramic membrane for oxygen separation," *Journal of Membrane Science*, 2018.

[23] D. F. Sanders et al., "Energy-efficient polymeric gas separation membranes for sustainable future: A review," *Polymer*, vol. 54, pp. 4729-4761, 2013.

[24] I. Pinnau and L. G. Toy, "Transport of organic vapors through poly(1-trimethylsilyl-1-propyne)," *Journal of Membrane Science*, vol. 116, pp. 199-209, 1996.

[25] C. A. Scholes, J. Jin, G. W. Stevens, and S. E. Kentish, "Hydrocarbon Solubility, Permeability and Competitive Sorption Effects in Polymer of Intrinsic Microporosity (PIM-1) Membranes," *Journal of Polymer Science, Part B: Polymer Physics*, vol. 54, pp. 397-404, 2016.

[26] L. Yu, M. Grahn, and J. Hedlund, "Ultra-thin MFI membranes for removal of C3+ hydrocarbons from methane," *Journal of Membrane Science*, vol. 551, pp. 254-260, 2018.

[27] S. Thomas, I. Pinnau, N. Du, and M. D. Guiver, "Hydrocarbon/hydrogen mixed-gas permeation properties of PIM-1, an amorphous microporous spirobisindane polymer," *Journal of Membrane Science*, vol. 338, pp. 1-4, 2009.

[28] R. B. Eldridge, "Olefin/Paraffin Separation Technology: A Review," *Ind. Eng. Chem. Res.*, vol. 32, pp. 2208-2212, 1993.

[29] T. C. Merkel et al., "Silver salt facilitated transport membranes for olefin/paraffin separations: Carrier instability and a novel regeneration method," *Journal of Membrane Science*, vol. 447, pp. 177-189, 2013.

[30] R. L. Burns and W. J. Koros, "Defining the challenges for C3H6/C3H8 separation using polymeric membranes," *Journal of Membrane Science*, vol. 211, no. 2, pp. 299-309, 2003.

[31] C. Zhang, Y. Dai, J. R. Johnson, O. Karvan, and W. J. Koros, "High performance ZIF-8/6FDA-DAM mixed matrix membrane for propylene/propane separations," *Journal of Membrane Science*, vol. 389, pp. 34-42, 2012.

[32] Y. H. Chu et al., "Iron-containing carbon molecular sieve membranes for advanced olefin/paraffin separations," *Journal of Membrane Science*, vol. 548, pp. 609-620, 2018.

[33] J. D. Figueroa, T. Fout, S. Plasynski, H. McIlvried, and R. D. Srivastava, "Advances in CO2 capture technology - The U.S. Department of Energy´s Carbon Sequestration Program," *International Journal of Greenhouse Gas Control* 2, pp. 9-20, 2008.

[34] T. J. Kim, H. Vralstad, M. Sandru, and M. B. Hagg, "Separation performance of PVAm composite membrane for CO2 capture at various pH levels," *Journal of Membrane Science*, vol. 428, pp. 218-224, 2013.

[35] K. A. Berchtold, R. P. Singh, J. S. Young, and K. W. Dudeck, "Polybenzimidazole composite membranes for high temperature synthesis gas separations," *Journal of Membrane Science*, pp. 265-270, 2012.

[36] D. Palanzo et al., "Evolution of the Extracorporeal Life Support Circuitry," *Artificial Organs*, vol. 34, no. 11, pp. 869-873, 2010.

[37] J. A. Potkay, "The promise of microfluidic artificial lungs," *Lab Chip*, vol. 14, pp. 4122-4138, 2014.

[38] M. Pflaum et al., "Endothelialization and characterization of titanium dioxide-coated gas-exchange membranes for application in the bioartificial lung," *Acta Biomaterialia*, vol. 50, pp. 510-521, 2017.

[39] Y. B. Wang, K. H. Shi, H. L. Jiang, and Y. K. Gong, "Significantly reduced adsorption and activation of blood components in a membrane oxygenator system coated with crosslinkable zwitterionic copolymer," *Acta Biomaterialia*, vol. 40, pp. 153-161, 2016.

[40] W. S. Wang and C. Wang, *Polyurethane for biomedical applications: A review of recent developments*.: Woodhead Publishing Reviews: Mechanical Engineering Series, 2012.

[41] D. J. Lyman, K. Knutson, and B. McNeil, "The effects of chemical structure and surface properties of synthetic polymers on the coagulation of blood. IV: The relationship between polymer morphology and protein adsorption," *Transactions of the American Society of Artificial Internal Organs*, vol. 21, pp. 49-53, 1975.

[42] M. D. Lelah, J. A. Pierce, L. K. Lambrecht, and S. L. Cooper, "Polyether-urethane monomers: Surface property/ ex vivo blood compatibility relationship," *Journal of Colloid Interface Science*, vol. 104, pp. 422-439, 1985.

[43] W. Ou, H. Qiu, Z. Chen, and K. Xu, "Biodegradable block poly(ester-urethane)s based on poly(3-hydroxybutyrate-co-4-hydroxybutyrate) copolymers," *Biomaterials*, vol. 32, pp. 3178-3188, 2011.

[44] A. Rashti et al., "Development of novel biocompatible hybrid nanocomposites based on polyurethane-silica prepared by sol gel process," *Materials Science and Engineering*, vol. 69, pp. 1248-1255, 2016.

[45] B. R. Barrioni, S. M. Carvalho, A. A. Oliveira, and M. M. Pereira, "Improved biocompatibility of polyurethane film by association with bioactive glass through ultrasonic implantation," *Materials Letters*, vol. 223, pp. 53-56, 2018.

[46] R. , Anderson, J. , McVenes, R. and Stokes, K. Ward, "In vivo biostability of polysiloxane polyether polyurethanes: Resistance to biologic oxidation and stress cracking," *Journal of Biomaterials Research A*, vol. 77A, pp. 580-589.

[47] K. E. Styan, D. J. Martin, A. Simmons, and L. A. Poole-Warren, "In vivo biostability of polyurethane-organosilicate nanocomposites," *Acta Biomaterialia*, vol. 8, no. 6, pp. 2243-2253, 2012.

[48] A. Solanski, M. Das, and S. Thakore, "A review on carbohydrate embedded polyurethanes: An emerging area in the scope of biomedical applications," *Carbohydrate Polymers*, vol. 181, pp. 1003-1016, 2018.

[49] C. T. Zhao and M. N. de Pinho, "Design of polypropylene oxide/polybutadiene bi-soft segment urethane/urea polymer for pervaporation membranes," *Polymer*, vol. 40, pp. 6089-6097, 1999.

[50] D. P. Queiroz and M. N. de Pinho, "Gas permeability of polypropylene oxide/polybutadiene bi-soft segment urethane/urea membranes," *Desalination*, vol. 145, pp. 379-383, 2002.

[51] D. P. Queiroz, M. N. de Pinho, and C. Dias, "ATR-FTIR studies of poly(propylene oxide)/polybutadiene bi-soft segment urethane/urea membranes," *Macromolecules*, vol. 36, pp. 4195-4200, 2003.

[52] D. P. Queiroz and M. N. de Pinho, "Structural characteristics and gas permeation properties of polydimethylsiloxane/poly(propylene oxide) urethane/urea bi-soft segment membranes," *Polymer*, vol. 46, pp. 2346-2353, 2005.

[53] M. Faria, V. Geraldes, and M. N. de Pinho, "Surface characterization of asymmetric bi-soft segment poly(ester urethane urea) membranes for blood oxygenation medical devices," *International Journal of Biomaterials*, vol. 2012, p. e376321, 2012.

[54] M. Faria, P. Brogueira, and M. N. de Pinho, "Sub-micron tailoring of bi-soft segment asymmetric polyurethane membrane surfaces with enhanced hemocompatibility properties," *Colloids and Surface B: Biointerfaces*, vol. 86, pp. 21-27, 2011.

[55] M. N. de Pinho, "Process of synthesis asymmetric polyurethane based membranes with hemocompatibility characteristics and membranes obtained by said process," US9181384B2, 2010.

[56] M. Faria, M. Rajagopalan, and M. N. de Pinho, "Tailoring bi-soft segment poly(ester urethane urea) integral asymmetric membranes for CO2 and O2 permeation," *Journal of Membrane Science*, vol. 387-388, pp. 66-75, 2012.

[57] M. Faria and M. N. de Pinho, "Phase segregation and gas permeation properties of poly(urethane urea) bi-soft segment membranes," *European Polymer Journal*, vol. 82, pp. 260-276, 2016.

[58] T. M. Eusébio, "Polyurethane urea membranes for membrane blood oxygenators: synthesis and gas permeation properties," Instituto Superior Técnico, 2017.

[59] M. Mulder, *Basic Principles of Membrane Technology*, 2nd ed.: Springer, 1996.

[60] R. M. Barrer and E. K. Rideal, "Permeation, diffusion and solution of gases in organic polymers," *Transactions of the Faraday Society*, vol. 35, 1939.

[61] S. W. Rutherford and D. D. Do, "Review of Time Lag Permeation Technique as a Method for Characterisation of Porous Media and Membranes," *Adsorption*, vol. 3, pp. 283-312, 1997.

[62] W. A. Rogers, R. S. Buritz, and D. Alpert, "Diffusion Coefficient, Solubility and Permeability for Helium in Glass," *Journal of Applied Physics*, vol. 25, no. 7, pp. 868-875, 1954.

[63] M. Al-Ismaily, J. G. Wijimans, and B. Kruczek, "A shortcut method for faster determination of permeability coefficient from time lag experiments," *Journal of Membrane Science*, vol. 423-424, pp. 165-174, 2012.

[64] B. Kruczek, H. L. Frisch, and R. Chapanian, "Analytical solution for the effective time lag of a membrane in a permeate tube collector in which Knudsen flow regime exists," *Journal of Membrane Science*, vol. 256, pp. 57-63, 2005.

[65] B. Kruczek, F. Shemshaki, S. Lashkari, R. Chapanian, and H. L. Frisch, "Effect of a resistance-free tank on the resistance to gas transport in high vacuum tube," *Journal of Membrane Science*, vol. 280, pp. 29-36, 2006.

[66] S. Lashkari, B. Kruczek, and H. L. Frisch, "General solution for the time lag of a single-tank receiver in the Knudsen flow regime and its implications for the receiver´s configuration," *Journal of Mmebrane Science*, vol. 283, pp. 88-101, 2006.

[67] S. Lashkari and B. Kruczek, "Effect of resistance to gas accumulation in multi-tank receivers on membrane characterization by the time lag method. Analytical approach for optimization of the receiver," *Journal of Membrane Science*, vol. 360, pp. 442-453, 2010.

[68] H. Strathmann, P. Scheible, and R. W. Baker, "A rationale for the preparation of Loeb-Sourirajan-type cellulose acetate membranes," *Journal of Applied Polymer Science*, vol. 15, pp. 811-828, 1971.

[69] W. Rasband, "ImageJ".

[70] V. K. Saini, M. L. Pinto, and J. Pires, "Synthesis and adsorption properties of micro/mesoporous carbon-foams prepared from foam-shaped sacrificial templates," *Materials Chemistry and Physics*, vol. 138, pp. 877-885, 2013.

[71] D. N. Gray, "Polymeric Membranes for Artificial Lungs," in *Polymeric Materials and Artificial Organs*, Charles G. Gebelein, Ed., 1984, vol. 256, pp. 151-162.

[72] F. Wiese, K. V. Peinemann, and S. P. Nunes, *Membranes for Artificial Lungs in Membranes for the Life Sciences, Chapter 2*.: Wiley-VCH Verlag GmbH & Co. KGaA, 2007.

[73] R. H. Perry and D. W. Green, *Perry´s Chemical Engineers´Handbook*, 7th ed.: McGraw-Hill, 1997.

11 Annex

11.1 Setup volume calibration

As a new cylinder (Cylinder 2) was added to the setup, it was necessary to do a volume calibration which was performed by gas expansion. Knowing the volume of the small cylinder (Cylinder 1), which was previously determined to be 12.6 ± 0.1 cm^3, it is simple to perform the calibration.

First, an impermeable membrane is inserted in the permeation cell to isolate the permeate side from the feed. After the temperature is stabilized at 25 ºC, the installation is pressurized with nitrogen with both cylinders and valve V1 and V2 opened and valve V3 closed. The cylinders and the valves V1 and V2 are then closed and the pressure P_1 is read. Then, valve V3 is opened and the setup is degassed. The pressure P_2 is registered after closing V3. In the following step, Cylinder 1 is opened and the pressure P_3 is obtained. Then, Cylinder 1 is closed and the installation is degassed again. After closing V3, the pressure P_2' is read and Cylinder 2 is opened, obtaining the pressure P_4.

After obtaining the pressures, the Ideal Gas Law is used to calculate the volumes. Considering that n_{12} is the sum of the number of moles in Cylinder 1 (n_1) and the number of moles in the tubes (n_2):

$$n_{12} = n_1 + n_2 \qquad (31)$$

And applying the Ideal Gas Law:

$$n = \frac{PV}{RT} \qquad (32)$$

We can obtain the following expression:

$$\frac{P_3 V_{12}}{RT} = \frac{P_1 V_1}{RT} + \frac{P_2 V_2}{RT} \qquad (33)$$

Considering that the temperature is constant and rearranging the equation, the following expression is obtained, allowing us to calculate the volume of the tubes (V_2):

$$V_2 = V_1 \frac{P_1 - P_3}{P_3 - P_2} \qquad (34)$$

The same can be applied to obtain the volume of Cylinder 2 (V_3):

$$V_3 = V_2 \frac{P_2' - P_4}{P_4 - P_1} \qquad (35)$$

The volumes of the tubes and Cylinder 2 obtained were 13.5 ± 0.01 cm^3 and 167.2 ± 0.2 cm^3, respectively, resulting in a total volume of the permeate side of 193.3 ± 0.3 cm^3.

The volumes were corrected with the virial coefficients for nitrogen and were found to make no difference.

11.2 Solubility measurements in the gas permeation setup by the barometric method

Solubility measurements of the poly(ester urethane urea) membranes by the barometric method were attempted by using the gas permeation setup, as it was done in the volumetric apparatus. A strip of membrane A31 was rolled, inserted in the permeation cell and degassed with the vacuum pump, keeping V1, V5 and V7 closed and the rest opened. The measurements were carried out at 37 ºC. After degassing, V3 was closed and CO_2 was introduced at a desired pressure by opening V1. After closing V6, the pressure was registered and the setup was degassed. Then, V3 was closed and V6 was opened, allowing the gas to expand through the setup and adsorb into the membrane. The pressure was registered after reaching an equilibrium. This procedure was repeated until an isotherm was obtained, as shown in red in Figure 30.

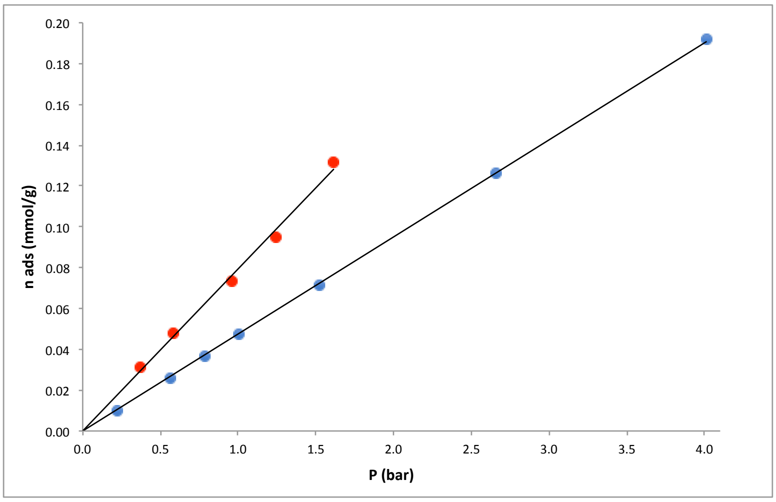

Figure 30 – CO_2 sorption isotherms obtained for membrane A31 at the gas permeation setup (red) and at the volumetric apparatus (blue)

The solubility coefficient obtained is 2.54x10^{-2} cm^3/cm^3.cmHg which is 29% higher than the value obtained at the volumetric apparatus, 1.98x10^{-2} cm^3/cm^3.cmHg, concluding that the gas permeation setup is unsuitable for this measurement. This error is probably due to the uncertainty of the calibrated volumes of the setup and the fact that the membrane adsorbs too little gas. Moreover, a stable temperature is required in these measurements as the pressure transmitter is very sensible to it, however, the fridge had to be opened to manipulate V6. The measurements might be improved by adding more membrane so that more gas is adsorbed and putting the valve V6 outside of the fridge, so that the temperature is not disturbed during measurements.

11.3 Early approximation method

The diffusion coefficients were determined by an alternative method to the time lag which is the early approximation method. From a permeation curve, a $\ln\left(\frac{Pp(t)}{\sqrt{t}}\right)$ vs $\frac{1}{t}$ plot was obtained, as shown in Figure 31, and a diffusion coefficient was acquired from the slope.

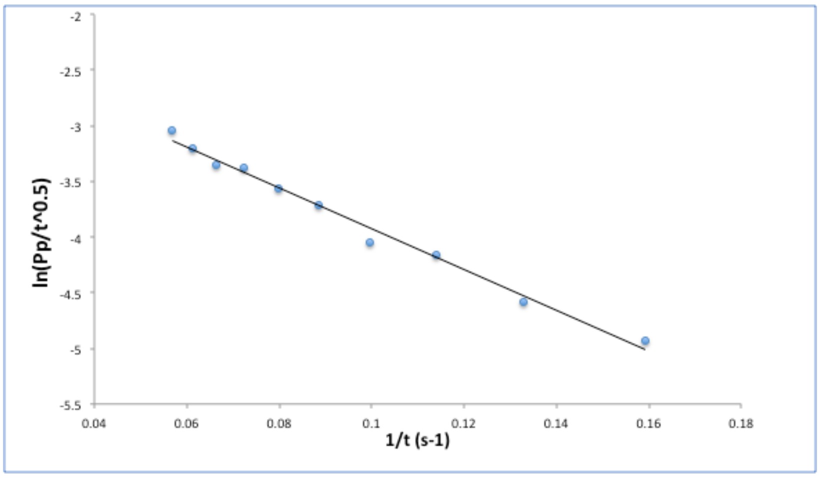

Figure 31 – $\ln\left(\frac{Pp(t)}{\sqrt{t}}\right)$ vs $\frac{1}{t}$ plot obtained from CO_2 permeation curve for membrane A31 at a feed pressure of 1.7 bar

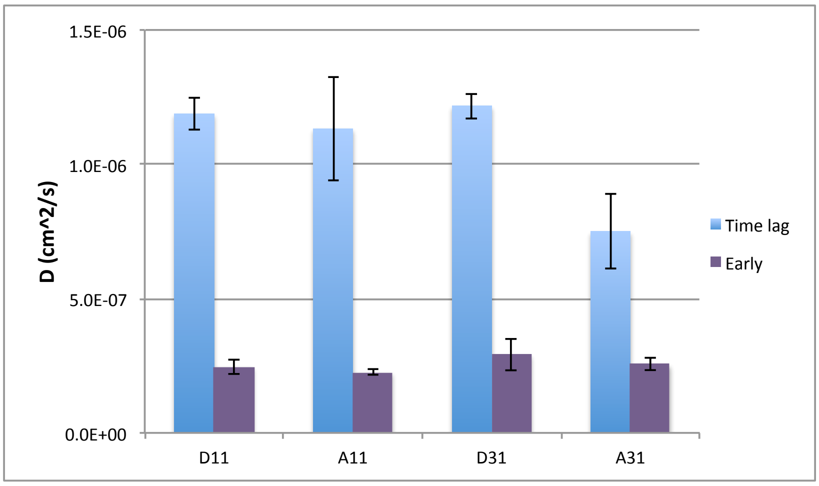

Figure 32 – Diffusion coefficients and respective standard deviations obtained for CO_2 for membranes A31, A11, D31 and D11 by the time lag and early approximation methods

Comparing both methods, the diffusion coefficients obtained by the early approximation method are much lower than the values obtained by the time lag method, corresponding to a relative error of 65-80%. A possible reason is that the time lags are too short, with a length of just a few seconds. Because this method is based on the transient state, it is probably more accurate for very impermeable membranes where the transient state is hours to weeks long. The time lag was thus chosen for the present work.